Hydrology and
Earth System
Sciences

Open Access

Evapotranspiration and water yield over China's landmass from 2000 to 2010

Y. Liu[1,2], Y. Zhou[1,3], W. Ju[1,2], J. Chen[1,2], S. Wang[4], H. He[4], H. Wang[4], D. Guan[5], F. Zhao[4], Y. Li[6], and Y. Hao[7]

[1]Jiangsu Provincial Key Laboratory of Geographic Information Science and Technology, Nanjing University, Nanjing, 210023, China
[2]International Institute for Earth System Sciences, Nanjing University, Nanjing, 210023, China
[3]School of Geographic and Oceanographic Sciences, Nanjing University, Nanjing, 210023, China
[4]Key Laboratory of Ecosystem Network Observation and Modeling, Institute of Geographic Sciences and Natural Resources Research, Chinese Academy of Sciences, Beijing, 100101, China
[5]Institute of Applied Ecology, Chinese Academy of Sciences, Shenyang, 110016, China
[6]Northwest Institute of Plateau Biology, Chinese Academy of Sciences, Xining, 810008, China
[7]Graduate University of Chinese Academy of Sciences, Beijing, 100049, China

Correspondence to: Y. Zhou (zhouyl@nju.edu.cn)

Abstract. Terrestrial carbon and water cycles are interactively linked at various spatial and temporal scales. Evapotranspiration (ET) plays a key role in the terrestrial water cycle, altering carbon sequestration of terrestrial ecosystems. The study of ET and its response to climate and vegetation changes is critical in China because water availability is a limiting factor for the functioning of terrestrial ecosystems in vast arid and semiarid regions. To constrain uncertainties in ET estimation, the process-based Boreal Ecosystem Productivity Simulator (BEPS) model was employed in conjunction with a newly developed leaf area index (LAI) data set, MODIS land cover, meteorological, and soil data to simulate daily ET and water yield at a spatial resolution of 500 m over China for the period from 2000 to 2010. The spatial and temporal variations of ET and water yield were analyzed. The influences of climatic factors (temperature and precipitation) and vegetation (land cover types and LAI) on these variations were assessed.

Validations against ET measured at five ChinaFLUX sites showed that the BEPS model was able to simulate daily and annual ET well at site scales. Simulated annual ET exhibited a distinguishable southeast to northwest decreasing gradient, corresponding to climate conditions and vegetation types. It increased with the increase of LAI in 74 % of China's landmass and was positively correlated with temperature in most areas of southwest, south, east, and central China. The correlation between annual ET and precipitation was positive in the arid and semiarid areas of northwest and north China, but negative in the Tibetan Plateau and humid southeast China. The national annual ET varied from 345.5 mm in 2001 to 387.8 mm in 2005, with an average of 369.8 mm during the study period. The overall rate of increase, 1.7 mm yr^{-1} ($R^2 = 0.18$, $p = 0.19$), was mainly driven by the increase of total ET in forests. During 2006–2009, precipitation and LAI decreased widely and consequently caused a detectable decrease in national total ET. Annual ET increased over 62.2 % of China's landmass, especially in the cropland areas of the southern Haihe River basin, most of the Huaihe River basin, and the southeastern Yangtze River basin. It decreased in parts of northeast, north, northwest, south China, especially in eastern Qinghai-Tibetan Plateau, the south of Yunnan Province, and Hainan Province. Reduction in precipitation and increase in ET caused vast regions in China, especially the regions south of Yangtze River, to experience significant decreases in water yield, while some sporadically distributed areas experienced increases in water yield. This study shows that the terrestrial water cycles in China's terrestrial ecosystems appear to have been intensified by recent climatic variability and human induced vegetation changes.

1   Introduction

The terrestrial hydrological cycle is essential for the functioning and sustainability of earth systems (Hutjes et al., 1998). Understanding its spatial and temporal variations and underlying driving factors are fundamental to predicting the response and feedback of terrestrial ecosystems to global changes. As one of the most important components within the terrestrial hydrological cycle, evapotranspiration (ET) links the hydrological, energy, and carbon cycles (Fisher et al., 2008; Jung et al., 2010). Globally, terrestrial ET processes consume more than 50 % of the solar radiation absorbed by the land surface (Trenberth et al., 2009), and affect precipitation by returning approximately 60% of the annual land precipitation back to the atmosphere (Koster et al., 2004; Oki and Kanae, 2006).

Previous studies have indicated that global warming might intensify the terrestrial hydrological cycle and cause more frequent floods and droughts (Meehl and Tebaldi, 2004; Huntington, 2006). Accurate estimation of the spatial and temporal variations in ET is critical for better understanding of the interactions between the atmosphere and land surface, and improving water resource management and drought assessment under climate change (Jung et al., 2010; Yuan et al., 2010; Fisher et al., 2011; Yan et al., 2012; Zeng et al., 2012). However, ET is one of the most difficult components of the terrestrial water cycle to estimate accurately because of land surface heterogeneity and numerous controlling factors, including climate, plant biophysics, soil properties, topography, and others (Dirmeyer et al., 2006; Mu et al., 2007; Yuan et al., 2010).

In situ measurements using weighing lysimeter, Bowen ratio, sap flow meters, eddy covariance and scintillometers are generally considered to be reliable for quantifying ET at site and landscape (over several kilometers) scales (Z. Li et al., 2009; Wang and Dickinson, 2012), but it is practically impossible to apply such methods at regional and global scales. Alternatively, remote sensing techniques are able to capture temporally continuous land surface information over large areas, thus providing an effective tool for retrieving the ground parameters that control ET (Ju et al., 2010; Yang et al., 2012). Remotely sensed surface parameters, such as leaf area index (LAI), land cover, clumping index, albedo, temperature and emissivity have been successfully used to estimate ET directly or to drive process based ET models (Yuan et al., 2010; Ryu et al., 2011).

Various ET estimation models that use remotely sensed data have been developed in recent decades, including surface energy balance models (Jiang and Islam, 1999; Su, 2002; Miralles et al., 2011; Anderson et al., 2012), empirical statistical models (Wang and Liang, 2008), physical models (Mu et al., 2007; K. Zhang et al., 2010) and water balance models (Cheng et al., 2011; Rodell et al., 2011; Sahoo et al., 2011; Zeng et al., 2012; Y. Q. Zhang et al., 2012). Recently, a large number of papers exist on the use of remotely sensed data to estimate ET, including several review papers (Courault et al., 2005; Verstraeten et al., 2008; Gowda et al., 2007; Z. Li et al., 2009; Wang and Dickinson, 2012).

Current ET estimates using remote sensing data are far from satisfactory due to uncertainties generated by model structure, inputs, parameterization schemes, and scaling issues (El Maayar and Chen, 2006; Yuan et al., 2010; Fernández-Prieto et al., 2012; Jia et al., 2012). Therefore it is essential to look for effective ways to constrain uncertainties in estimating ET using remote sensing data. Given the rapid development of remote sensing techniques, improving capacity of computation and storage, and increasing availability of ET measurements in recent years (Mu et al., 2011; Ryu et al., 2011; Sasai et al., 2011), it is now feasible to improve ET estimation by improving the spatial resolution of inputs and model structure (Ryu et al., 2011; Vinukollu et al., 2011), and by optimizing model parameters.

The climate of China is diverse and complex, ranging from tropical to cold-temperate, and from humid to extremely dry (Mu et al., 2008; Piao et al., 2010, 2011). Severe droughts and floods frequently impact ecosystems (Liu et al., 2008). In the past decade, the earth has experienced the most significant increase in temperature since instrumental measurements began (Trenberth et al., 2007; Zhao and Running, 2010). In parallel to the global increases, China also experienced significant increases in mean annual temperature (MAT), changes in seasonal and interannual patterns of precipitation during the past two decades (Fang et al., 2010; Piao et al., 2011), and more frequently severe droughts (Gao and Yang, 2009; Piao et al., 2009; Qin et al., 2010; Lu et al., 2011; Wang et al., 2011). Studies showed that drying and warming (Ma and Fu, 2006; Piao et al., 2010) intensified the hydrological cycle in western China, but weakened in north of the Yellow River basin (Gao et al., 2007) in the past half century. Several extensively unusual droughts have hit China since 2000, how the terrestrial water cycle respond to these climatic extremes has not been thoroughly investigated yet.

The terrestrial water cycle is also significantly affected by land cover change, which has been dramatic in China. Several large-scale forest plantations programs have been implemented by Chinese government since the late 1970s for environment protection and vegetation restoration (Cao et al., 2011; Yu et al., 2011; Huang et al., 2012; Piao et al., 2012), thus increasing forested area from 2000 to 2010 (FAO, 2010; Piao et al., 2012). Meanwhile, urbanization has been intensive (Li et al., 2011; J. Y. Liu et al., 2012; Wang et al., 2012). Inevitably, human intervention and climate change must alter China's terrestrial water cycle (Piao et al., 2007).

Recently, several studies have been conducted to quantify spatio-temporal variations of ET in China using various methods, such as pan evaporation observations and ecosystem models driven by remote sensing data (Liu et al., 2008; Zhou et al., 2009; Zhu et al., 2010; M. L. Liu et al., 2012; Li et al., 2012). However, most ET calculations were implemented at relatively coarse resolutions, such as 10 km, and

did not fully make use of remote sensing data. In addition, there are very few studies on water yield changes in terrestrial ecosystems of the country. This suggests that a more thorough investigation of ET and water yield incorporating land surface information retrieved from remote sensing should be carried out to better understand the terrestrial water cycle response to recent changes in climate and vegetation.

In order to constrain the uncertainties, daily ET and water yield were simulated at a spatial resolution of 500 m using an improved LAI data set and the process-based BEPS (Boreal Ecosystem Productivity Simulator) model. Spatial and temporal variations of ET and water yield in different regions of China during the 2000–2010 period were then analyzed, resulting in identification of the major factors driving the variations. The main objectives are to (1) evaluate the ability of the BEPS model to simulate ET in different ecosystems of China; (2) analyze the spatial and temporal patterns of ET and water yield in its terrestrial ecosystems from 2000 to 2010; (3) assess the roles of temperature, precipitation and LAI in regulating ET over the country.

2   Methods and data

2.1   The BEPS model

The Boreal Ecosystem Productivity Simulator (BEPS) is a process-based terrestrial ecosystem model designed to simulate carbon, water, and energy budgets at continental or landscape scale (Liu et al., 1997, 1999; Chen et al., 1999). One of the unique characteristics of this model is tight coupling between remote sensing information, and water and carbon cycle processes. The BEPS is driven by spatially explicit data sets from meteorology, remotely sensed land surface parameters such as LAI and land cover type, and soil texture (Liu et al., 1999, 2003). This model includes a sunlit and shaded leaf separation photosynthesis module for calculating carbon fixation, and an energy balance and hydrological module for simulating evapotranspiration (ET) and soil water content dynamics, as well as a soil biogeochemical module for simulating soil carbon and nitrogen dynamics. The photosynthesis module is developed on the basis of Farquhar's instantaneous leaf biochemical model (Farquhar et al., 1980), with a new spatial and temporal scaling scheme (Chen et al., 1999), to calculate daily carbon fixation by the canopy. Water and carbon cycles are coupled through leaf stomatal conductance that is controlled by environmental factors, which include photosynthetic photon flux density, temperature, vapor pressure deficit, and soil water content (Jarvis, 1976). Although initially developed to estimate gross and net primary productivity for boreal ecosystems in Canada, the BEPS model has been used elsewhere (Ju et al., 2006; Chen et al., 2007; Sonnentag et al., 2008; Govind et al., 2009a,b), and successfully applied to estimate regional water and carbon fluxes in China (Sun et al., 2004; Wang et al., 2005; Feng et al., 2007;

Zhou et al., 2009; Ju et al., 2010; Liu et al., 2013), East Asia (Matsushita and Tamura, 2002; F. Zhang et al., 2010; Zhang et al., 2012b), North America (Liu et al., 1999; Ju et al., 2006; Sonnentag et al., 2008; Sprintsin et al., 2012; Zhang et al., 2012a), Europe (Wang et al., 2004) and across the globe (Chen et al., 2012).

The BEPS model has shown strong performances in several model intercomparison studies that evaluated ecosystem models against carbon and water flux measurements (Amthor et al., 2001; Potter et al., 2001; Grant et al., 2005, 2006; Schwalm et al., 2010; Schaefer et al., 2012). In an intercomparison among nine models, for example, the BEPS produced the second lowest RMSE (root mean square error) for ET simulation over a boreal forest (Amthor et al., 2001). In a recent North American carbon program study, the BEPS RMSE was the eighth lowest among 24 models used in gross primary productivity simulation (Schaefer et al., 2012).

2.1.1   ET calculation

In the BEPS model, ET from terrestrial ecosystems is calculated as

$$\mathrm{ET} = T_{\mathrm{plant}} + E_{\mathrm{plant}} + S_{\mathrm{plant}} + E_{\mathrm{soil}} + S_{\mathrm{ground}}, \qquad (1)$$

where T_{plant} is transpiration from the canopy, E_{plant} and E_{soil} are the respective evaporation of intercepted precipitation and soil surface, S_{plant} and S_{ground} are respective snow sublimation from the canopy and ground surface.

Canopy transpiration is further calculated as

$$T_{\mathrm{plant}} = T_{\mathrm{plant,sun}} \, \mathrm{LAI}_{\mathrm{sun}} + T_{\mathrm{plant,shaded}} \, \mathrm{LAI}_{\mathrm{shaded}}, \qquad (2)$$

where $T_{\mathrm{plant,sun}}$ and $T_{\mathrm{plant,shaded}}$ are the transpiration from per unit area of sunlit and shaded leaves, $\mathrm{LAI}_{\mathrm{sun}}$ and $\mathrm{LAI}_{\mathrm{shaded}}$ are respective the LAI of the sunlit and shaded leaves, partitioned according to total canopy LAI, daily mean solar zenith angle, θ, and clumping index, Ω (Chen et al., 1999).

Transpiration from sunlit and shaded leaves is calculated from the Penman–Monteith equation (Monteith, 1965):

$$T_{\mathrm{plant},j} = \frac{\Delta R_{\mathrm{n},j} + \rho c_p \, \mathrm{VPD}/r_{\mathrm{a}}}{\left(\Delta + \gamma \left(1 + r_{\mathrm{s},j}/r_{\mathrm{a}} \right) \right) \lambda v}, \qquad (3)$$

where the j subscript denotes sunlit or shaded leaves; Δ is the slope of the saturated water vapor pressure curve ($\mathrm{kPa}\,^{\circ}\mathrm{C}^{-1}$); $R_{\mathrm{n},j}$ is the net radiation ($\mathrm{W\,m}^{-2}$); ρ is the air density ($\mathrm{kg\,m}^{-3}$); c_p is the specific heat of air ($\mathrm{J\,kg}^{-1}\,^{\circ}\mathrm{C}^{-1}$); γ is the psychrometric constant ($\mathrm{kPa}\,^{\circ}\mathrm{C}^{-1}$); r_{a} is the aerodynamic resistance ($\mathrm{s\,m}^{-1}$) assigned according to land cover types (Liu et al., 2003); and $r_{\mathrm{s},j}$ is the sunlit or shaded leaf stomatal resistance ($\mathrm{s\,m}^{-1}$).

E_{soil} is also calculated from the Penman–Monteith equation; the resistance of the soil surface changing with the degree of saturation in the first soil layer (Ju et al., 2010). E_{plant}, S_{plant}, and S_{ground} are computed following Liu et al. (2003).

2.1.2 Stomatal resistance calculations

Stomatal resistance of sunlit and shaded leaves is determined from the Jarvis model (Jarvis, 1976):

$$r_j = r_{\min} f(T) f(\text{VPD}) f\left(\text{PPFD}_j\right) f(W), \tag{4}$$

where j denotes sunlit or shaded leaf, $r_{\min}$ is the minimum stomatal resistance (s m^{-1}) assigned according to land cover types; and $f(T)$, $f(\text{VPD})$, $f(\text{PPFD}_j)$, and $f(W)$ are the respective scalars that quantify the effects of temperature, atmospheric vapor pressure deficit, photosynthetic photon flux density and soil water content on stomatal resistance.

Considering that vegetation is able to optimize the uptake of soil water, the soil water scalar $f(W)$ in Eq. (4) is

$$f(W) = \sum_{i=1}^{n} f_{w,i}\, \beta_i, \tag{5}$$

where $f_{w,i}$ is the soil water stress factor in layer i, and β_i is the weight of layer i expressed as a function of soil water availability and root abundance (Ju et al., 2006):

$$\beta_i = \frac{r_i f_{w,i}}{\sum\limits_{i=1}^{n} r_i f_{w,i}}, \tag{6}$$

in which r_i is the root fraction within layer i, determined according to Zhang and Wegehenkel (2006).

In Eq. (6), the term $f_{w,i}$ in layer i is calculated as (Chen et al., 2005; Ju et al., 2010):

$$f_{w,i} = \begin{cases} \max\left[0.25, 2\left(\frac{\theta_i - \theta_{w,i}}{\theta_{f,i} - \theta_{w,i}}\right) - \left(\frac{\theta_i - \theta_{w,i}}{\theta_{f,i} - \theta_{w,i}}\right)^2\right] & \theta_i \le \theta_{f,i} \\ 1 - 0.4\left(\frac{\theta_i - \theta_{f,i}}{\theta_{s,i} - \theta_{f,i}}\right) & \theta_i > \theta_{f,i} \end{cases}, \tag{7}$$

where θ_i is the simulated volumetric soil water content in layer i, and $\theta_{w,i}$, $\theta_{f,i}$ and $\theta_{s,i}$ are, respectively, the wilting point, field capacity and porosity of soil layer i. They are determined according to the fractions of clay, silt and sand (Saxton et al., 1986).

2.1.3 Soil water content simulation

Originally, the BEPS used a bucket model approach to simulate soil water content (Liu et al., 2003). In this study, the soil profile was stratified into three layers with thicknesses of 0.1, 0.25, and 0.85 m. Soil evaporation is limited to the first soil layer, while vegetation can take up water from all three layers through transpiration. Therefore, the changes of soil water content in three soil layers are simulated as

$$\frac{\partial \theta_1}{\partial t} = \frac{1}{d_1}\left[P_{\text{gs}} - T_{\text{plant},1} - E_{\text{s}} - \text{RF} - Q_{1,2}\right] \tag{8}$$

$$\frac{\partial \theta_2}{\partial t} = \frac{1}{d_2}\left[Q_{1,2} - T_{\text{plant},2} - Q_{2,3}\right] \tag{9}$$

$$\frac{\partial \theta_3}{\partial t} = \frac{1}{d_3}\left[Q_{2,3} - T_{\text{plant},3} - Q_3\right], \tag{10}$$

where $\theta_{i=1,3}$ is the water content of soil layer i for $i = 1$, 3; $d_{i=1,3}$ is the soil layer thickness (m); P_{gs} is precipitation throughfall at the ground surface (m d^{-1}); $T_{\text{plant},i=1,3}$ is the transpiration uptake from a soil layer (m d^{-1}); E_{s} is the evaporation loss from the soil surface (m d^{-1}); RF is the surface runoff estimated as a function of P_{gs} and θ_1; $Q_{i,i+1}$ is the vertical exchange of soil water between adjacent soil layers $i = 1$, 2 and $i + 1$ (m d^{-1}); and Q_3 is the saturated subsurface flow from layer 3 out of the soil profile, calculated according to soil water content and saturated hydraulic conductivity.

The flux of soil water between adjacent layers i and $i + 1$ is simulated from (Sellers et al., 1996):

$$Q_{i,i+1} = \frac{k_i d_i + k_{i+1} d_{i+1}}{d_i + d_{i+1}}\left(1 + 2\frac{w_i - w_{i+1}}{d_i + d_{i+1}}\right), \tag{11}$$

where k_i and k_{i+1} are the respective hydraulic conductivities (m d^{-1}) in soil layers i and $i + 1$; w_i and w_{i+1} are the corresponding water potential (m).

The hydraulic conductivity of a soil layer is calculated as

$$k_i = K_i \left(\frac{\theta_i}{\theta_{s,i}}\right)^{2b+3}, \tag{12}$$

where K_i is the saturated hydraulic conductivity of soil layer (m d^{-1}); and b is a soil texture dependent parameter used to determine the rate of hydraulic conductivity changing with soil water content.

2.2 Model input data

The BEPS model uses both spatially distributed and static data sets as inputs. Atmospheric CO_2 concentration is assumed to be well mixed and spatially homogenous. The spatially distributed inputs listed in Table 1 include: (1) land cover maps, (2) LAI time series, (3) daily meteorological data, and (4) soil texture. Prior to simulation, all spatially explicit input data set inputs were projected onto an Albers conical equal area projection at a spatial resolution of $500\,\text{m} \times 500\,\text{m}$.

2.2.1 LAI data

A data set of 8-day LAI at 500 m resolution for the period from 2000 to 2010 was generated using an inversion algorithm based on the 4-scale geometrical optical model (Deng et al., 2006). This LAI inversion algorithm was driven by the MODIS MCD12Q1 V051 land cover (Friedl et al., 2010) and MOD09A1 V05 reflectance products. It is based on relationships between LAI and vegetation indices that were simulated by the 4-scale geometrical optical model with corrections for the effects of changes in sun and sensor angles on reflectance and vegetation indices (Chen and Leblanc, 1997). Due to proven superiority over the MODIS LAI algorithm in applications to work in Canada, China, and other regions (Liu et al., 2007; Pisek et al., 2007; X. Li et al., 2009; Y. Liu

Table 1. BEPS input data sets and their description.

Data	Description	Original resolution	Period	Source
LAI data	8-day LAI derived from MODIS land cover and reflectance (MOD09A1 V05) products	500 m	2000–2010	This study
Land cover data	Annual MODIS land cover data set (MCD12Q1 V051)	500 m	2001–2010	Friedl et al. (2010)
Meteorological data	Daily maximum and minimum temperatures, relative humidity, sunshine duration, and precipitation	500 m	2000–2010	This study
Soil data	Soil texture spatial maps (volumetric percentages of clay, sand, and silt components)	1 km	Average	Shangguan et al. (2012)

et al., 2012), the LAI inversion algorithm has been adopted by the European Space Agency GLOBCARBON project to generate a global LAI product. The inverted LAI was further smoothed using a locally adjusted cubic-spline capping (LACC) method (Chen et al., 2006) to remove unrealistic fluctuations caused by residual cloud contamination and atmospheric noises.

2.2.2 Land cover data

The annual MODIS land cover data set, MCD12Q1 V051, from 2001 to 2010 at a spatial resolution of 500 m (Friedl et al., 2010), was used to assign plant physiological parameters required in the LAI inversion algorithm and BEPS model. Owing to the deficiency of MODIS land cover data in 2000, the MODIS land cover data set of 2001 was used as a surrogate for 2000 with an assumption that the change of land cover in two adjacent years was small. The Collection 5 land cover product has been substantially improved in spatial resolution and classification algorithm in comparison to that of Collection 4 (Friedl et al., 2010). It was generated using a regression tree method in combination with MODIS reflectance in bands 1 to 7, albedo, land-surface temperature, texture, and other characteristics (Friedl et al., 2002, 2010). Errors in the land cover type data set will cause uncertainties in calculated ET and water yield because different land cover types have different transpiration capacity. In the MCD12Q1 V051 product, there are five different land cover data sets corresponding to different classification systems. In this study, the data set generated using the IGBP land cover classification system was used (Loveland and Belward, 1997), and further aggregated into ten groups of vegetation cover type (Fig. 1), including evergreen needleleaf forest (ENF), evergreen broadleaf forest (EBF), deciduous needleleaf forest (DNF), deciduous broadleaf forest (DBF), mixed forest (MF), shrubland (SHR), grassland (GRA), cropland (CRO), cropland/natural vegetation mosaic (NAV), and non-vegetation (NOV).
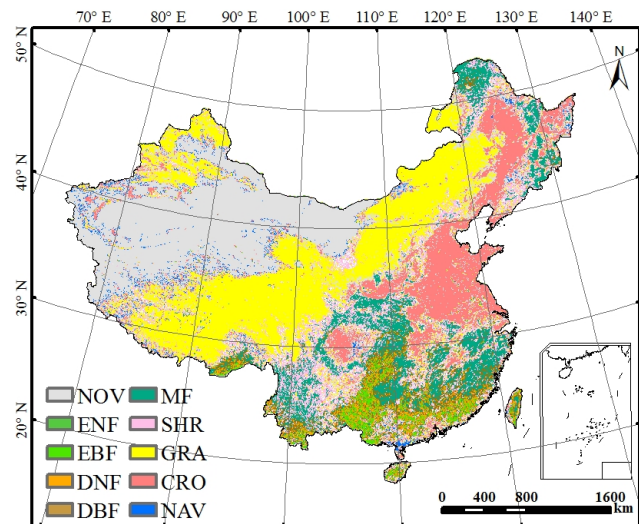
Fig. 1. Land cover map of China in 2010 derived from the MODIS land cover data set: ENF – evergreen needleleaf forest; EBF – evergreen broadleaf forest; DNF – deciduous needleleaf forest; DBF – deciduous broadleaf forest; MF – mixed forest; SHR – shrubland; GRA – grassland; CRO – cropland; NAV – cropland/natural vegetation mosaic; NOV – non-vegetation.

2.2.3 Meteorological data

Daily meteorological data, including maximum and minimum air temperatures, relative humidity, sunshine duration, and precipitation observed at 753 national basic meteorological stations in China were used to generate 500 m resolution meteorological fields for the 2000–2010 period using the inverse distance weighted interpolation method (Fig. 2). Incoming solar radiation required by the BEPS model was observed at only 102 meteorological stations in China, so it was calculated from observed daily sunshine duration. A lapse rate of 6 °C per 1000 m was assumed for the interpolation of temperatures. There was no meteorological data available for Taiwan province, and meteorological stations were sparse in northwestern areas, such as Xinjiang, Qinghai-Tibetan Plateau (Fig. 2). Such limited meteorological observations in

Table 2. ChinaFlux sites at which ET data were used for validating the BEPS model.

| Sites (abbreviation)	Changbaishan forest site (CBS)	Qianyanzhou forest site (QYZ)	Haibei grassland site (HB)	Xilinhot grassland site (XLHT)	Yucheng cropland site (YC)
Location	42°24′ N, 128°06′ E	26°44′ N, 115°03′ E	37°40′ N, 101°20′ E	43°33′ N, 116°40′ E	36°49′ N, 116°34′ E
Vegetation	Temperate deciduous broad-leaved and coniferous mixed forest	Typical subtropical monsoon man-planted forest	Alpine meadow	Temperate Leymus chinensis	Winter wheat and summer maize
Soil type	Mountain dark brown soil	Typical red earth	Alpine meadow soil	Chernozem soil	Aquox and salt aquox
Elevation/m	736	100	3293	1189	23
Mean annual temperature/°	4.0	17.9	−1.4	−0.4	13.1
Annual precipitation/mm	695	1485	580	350–450	528
LAI	6.1 (maximum in grown season)	3.6	2.8 (maximum in grown season)	1.5 (maximum in grown season)	
Type of EC sensors	Open-path IRGA (LI-7500) and 3-D sonic anemometers (CSAT3)	Open-path IRGA (LI-7500) and 3-D sonic anemometers (CSAT3)	Open-path IRGA (LI-7500) and 3-D sonic anemometers (CSAT3)	Open-path IRGA (LI-7500) and 3-D sonic anemometers (CSAT3)	Open-path IRGA (LI-7500) and 3-D sonic anemometers (CSAT3)
Period	2003, 2004	2003, 2004	2003	2004	2003, 2004
Reference	Wen et al. (2003); Zhang et al. (2011a)	Liu et al. (2006); Wen et al. (2006)	Li et al. (2005); Li et al. (2007)	Li et al. (2005); Zhang et al. (2011a)	Qin et al. (2005); Li et al. (2006)

these areas would inevitably induce uncertainties in interpolated meteorological data, and consequently in simulated ET and water yield.

2.2.4 Soil data

Soil texture maps generated from the 1 : 1 000 000 scale soil map of China and 8595 soil profiles recorded in the second national soil survey data set developed by Shangguan et al. (2012), were also interpolated to a spatial resolution of 500 m to drive the BEPS model. The soil texture, represented by the volumetric percentages of clay, sand and silt components, was used to estimate hydrological parameters, such as water potential at the wilting point (1500 kPa) and at field capacity (33 kPa), porosity, saturated hydrological conductivity and air entry water potential.

2.3 Model validation

The performance of the BEPS model to simulate ET flux has previously been validated by using measurements in North America (Liu et al., 2003), East Asia (F. Zhang et al., 2010) and China (Wang et al., 2005). Here, it was further evaluated using ET measured by eddy covariance (EC) at five ChinaFLUX sites (Yu et al., 2006): (1) the Changbaishan temperate broad-leaved Korean pine mixed forest (CBS), (2) Qianyanzhou subtropical coniferous plantation (QYZ), (3) Haibei alpine meadow (HB), (4) Xilinhot temperate steppe (XLHT), and (5) Yucheng warmer temperate cropland (YC) which are identified in Fig. 2, with detailed information listed in Table 2. ET measured every 30 min was aggregated into daily values, termed observed ET hereafter, for model validation. The EC systems consisted of open-path infrared gas analyzers (Model LI-7500, LICOR, Lincoln, Nebraska, USA) and 3-D sonic anemometers (Model
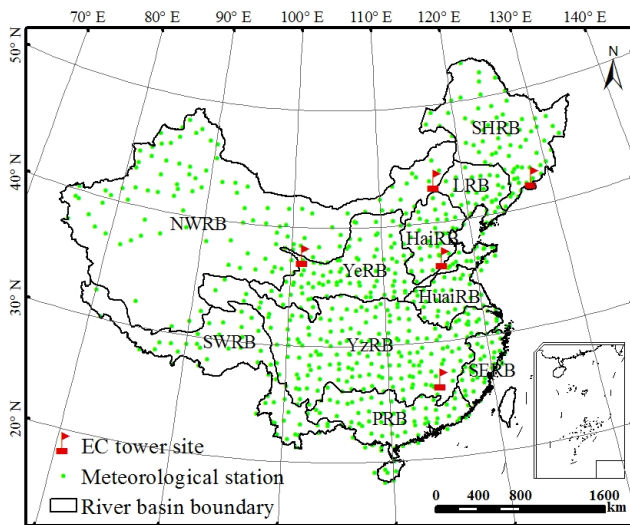
Fig. 2. Locations of flux tower sites (red flags), 753 national basic meteorological stations (green circles), and boundaries of 10 river basins (black lines): SHRB – Songhua River basin; LRB – Liaohe River basin; HaiRB – Haihe River basin; YeRB – Yellow River basin; HuaiRB – Huaihe River basin; YzRB – Yangtze River basin; SERB – southeast river basin; PRB – Pearl River basin; SWRB – southwest river basin; NWRB – northwest river basin.

CSAT3, Campbell Scientific Inc., Logan, Utah, USA). The instruments signals were recorded at 10 Hz on a datalogger (Model CR5000, Campbell Scientific Inc., Logan, Utah, USA) and block averaged over 30 min intervals for analyses and archiving.

For better analysis of ET and water yield spatial variations, the mainland of China is divided into 10 major river basins according to basin depiction in the hydrological yearbook of China (Fig. 2). They are the Songhua (SHRB), Liaohe (LRB), Haihe (HaiRB), Yellow (YeRB), Huaihe (HuaiRB), Yangtze (YzRB), Southeast (SERB), Pearl (PRB), Southwest (SWRB), and Northwest (NWRB). Annual water yield is calculated as the difference between annual precipitation input and ET output (Sun et al., 2005; Liu et al., 2008; Zhang et al., 2009; Vinukollu et al., 2011; M. L. Liu et al., 2012).

2.4 Accuracy assessment and trend analysis

Three metrics: coefficient of determination (R^2) of daily simulated and observed ET values, and the absolute predictive error (APE) and relative predictive error (RPE) of annual values, derived as the sum of daily values for each year, were used to evaluate the performance of the BEPS model in simulating ET. APE and RPE are calculated as

$$\text{APE} = \text{ET}_s - \text{ET}_o, \tag{13}$$

$$\text{RPE} = \left[\left(\text{ET}_s - \text{ET}_o \right) / \text{ET}_o \right] \times 100\%, \tag{14}$$

where ET_s and ET_o are, respectively, the simulated and observed annual ET.

Linear regression was used to analyze the temporal trends of the hydrological variables, ET and water yield, mean annual temperature (MAT), annual precipitation, and annual mean LAI between 2000 and 2010 (Y. Liu et al., 2012).

Three simulations were conducted here. In Simulation I, dynamic climate, LAI, and land cover during the 2000–2010 period were used to drive the BEPS. The spatial and temporal variations of ET and water yield and their linkages with climate and vegetation factors were analyzed on the basis of the outputs from this simulation scenario. In Simulation II, climate averaged over the 1980–2000 period, dynamic LAI and land cover over the 2000–2010 period were used to drive the BEPS model to investigate the effect of climatic variability on ET. In Simulation III, the BEPS model was driven by the land cover map in 2001 and dynamic climate and LAI over the 2000–2010. The purpose of this study was to assess the role of land cover change in regulating ET.

3 Results and discussion

3.1 BEPS model evaluation

Seasonal variations of simulated and observed daily ET at five ChinaFLUX sites are plotted in Fig. 3. Overall, the BEPS model was able to capture the seasonality of ET well. However, it tended to overestimate daily ET in autumn at the YC cropland site and underestimate the daily ET in spring at the HB grassland site. The regression line between simulated and observed daily ET was very close to 1 : 1 line at all sites, with slopes ranging from 0.84 to 1.05 and intercepts smaller than 0.10 (Table 3). The R^2 values of simulated daily ET against observations were mostly above 0.60 at these sites. However, the BEPS model performed relatively poorly in simulating ET at the YC site, with R^2 equal to 0.61 and 0.44 in 2003 and 2004, respectively. Two rotation crops, winter wheat and summer maize, were cultivated at this crop site. The overestimation of simulated ET mainly occurred in the growing seasons of summer maize. It was mainly caused by the simplified parameterization scheme for cropland in the BEPS model. The same parameter values were used for different crops due to the difficulty in obtaining reliable spatial distribution data of different crop types. This simplification might induce uncertainties in simulated ET for some crop species. Some studies have proved that the maximum stomatal conductance of summer maize is usually lower than that of winter wheat (Kelliher et al., 1995; Bunce, 2004). In this study, one maximum stomatal conductance was used to calculate ET for summer maize and winter wheat, resulting in overestimation of ET in the growing seasons of summer maize. When data at all sites lumped together, the BEPS model explained a significant proportion of the variation ($R^2 = 0.66$, $p < 0.0001$) in the daily ET (Fig. 4).

Annual simulated ET matched the observed ET well (Table 3). The RPE of simulated annual ET was in the range
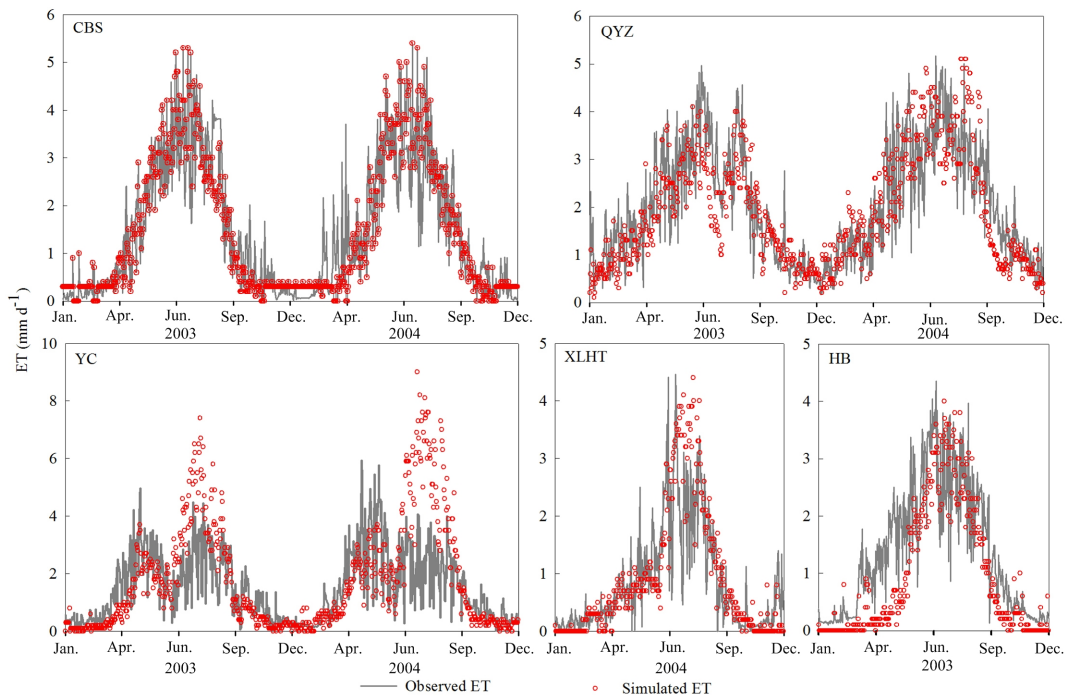
Fig. 3. Time series of observed and simulated daily ET (mm d^{-1}) from 2003 to 2005 at CBS, QYZ, YC, from 2004 to 2005 at XLHT, and from 2003 to 2004 at HB. Site information is stated in Table 2.
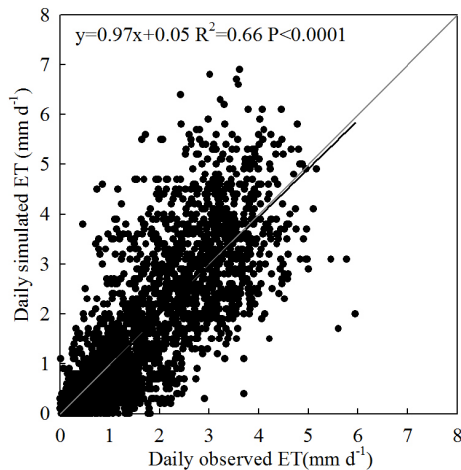
Fig. 4. Comparison between simulated and observed ET (mm d^{-1}) at all five tower sites.

of ±10 % at the CBS, QYZ, XLHT, and YC sites. However, RPE was −27.73 % at the HB site in 2003, mainly due to the underestimation of ET in the spring.

3.2 Spatial patterns of simulated ET and water yield

3.2.1 Spatial patterns of simulated annual ET

Figure 5a shows the spatial patterns of simulated ET in terrestrial ecosystems of China averaged over the period from 2000 to 2010. There were obviously identical spatial variations in mean annual ET relating to climate and vegetation types, with a decreasing trend from the southeast to the northwest. The spatial patterns of ET identified here are consistent with the findings from previous studies (Liu et al., 2008; Zhou et al., 2009; Xiao et al., 2013). Overall, ET was high in regions with widely distributed tropical evergreen forests, such as the PRB and SERB (Fig. 2). It was low in the NWRB of northwestern China. Mean annual ET in the YzRB, HuaiRB, PRB and SERB was normally above 500 mm yr^{-1}. In the PRB and SERB, mean annul ET was even above 700 mm yr^{-1}. ET showed an increasing trend from the upstream to the downstream areas within the YzRB, where it ranged from 200 to 400 mm yr^{-1} in upstream areas such as southern Qinghai and eastern Sichuan provinces, from 500 to 700 mm yr^{-1} in the middle stream areas, and more than 700 mm yr^{-1} in the downstream regions. Mean annual ET exhibited significant heterogeneity in the SWRB, where it was lower than 150 mm yr^{-1} in western Tibet, ranged from 200 to 300 mm yr^{-1} in central Tibet, and varied from 600 to 800 mm yr^{-1} in southeastern Tibet and southern Yunnan Province.

In northern China, mean annual ET decreased from east to west. Mean annual ET in the SHRB and LRB was about 600 mm yr^{-1} in forest areas, and 300 mm yr^{-1} in cropland and grassland areas. Similar linkage of ET with land cover types also occurred in the YeRB. The HaiRB is dominantly covered by croplands, and here the mean annual ET was

Table 3. Statistics of simulated and observed daily and annual ET at the five flux tower sites.

Site	Year	R^2	RMSE (mm d^{-1})	a^*	b^*	Observed ET (mm yr^{-1})	Simulated ET (mm yr^{-1})	APE (mm yr^{-1})	RPE (%)
CBS	2003	0.78	0.70	0.99	0.08	537.8	563.3	25.5	4.74
	2004	0.72	0.80	1.05	0.03	524.4	563.9	39.5	7.53
QYZ	2003	0.63	0.73	0.84	0.32	709.4	716.3	6.9	0.97
	2004	0.70	0.85	1.02	0.13	772.4	837.3	64.9	8.40
HB	2003	0.72	0.74	0.86	0.21	499.1	360.7	−138.4	−27.73
XLHT	2004	0.67	0.63	0.98	0.07	311.1	331.0	19.9	6.40
YC	2003	0.61	0.89	0.99	0.08	541.7	509.5	−32.2	−5.9
	2004	0.44	1.31	0.90	0.28	581.9	628.1	46.2	7.94

Note: R^2 = coefficient of determination; RMSE = root mean square error; APE = absolute predictive error; RPE = relative predictive error;
* $y = ax + b$, y and x denote simulated and observed daily ET, respectively.
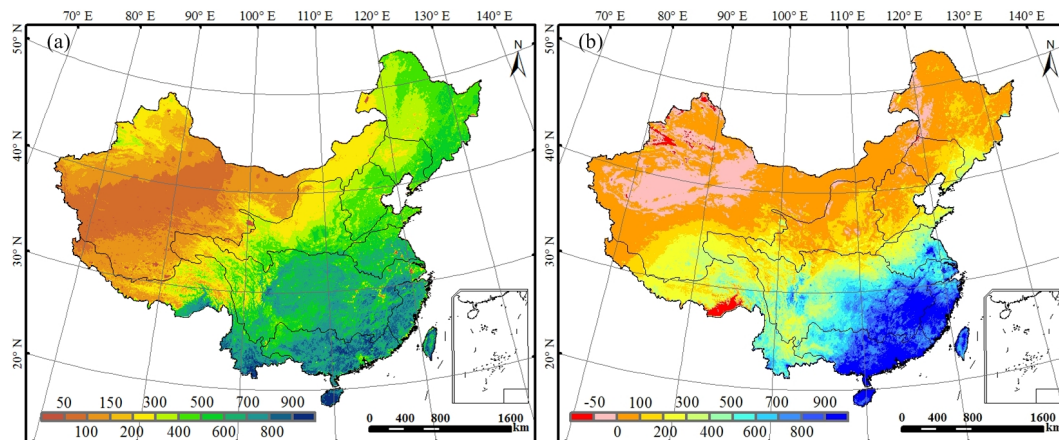
Fig. 5. The spatial distribution of **(a)** mean annual ET (mm yr^{-1}) and **(b)** water yield (mm yr^{-1}) from 2000 to 2010.

close to 500 mm yr^{-1}, in contrast to the arid NWRB, where mean annual ET was normally less than 150 mm yr^{-1} due to limited water supply and sparse vegetation.

Averaged over the basin scale, annual ET was highest in the PRB, at 729 mm, followed by those in the SERB (714 mm), HuaiRB (568 mm) and YzRB (552 mm). The average ET was lowest in the NWRB (144 mm yr^{-1}), next lowest in the YeRB (349 mm yr^{-1}). The totals of ET within individual basins ranged from 106.28 km^3 in the LRB to 986.79 km^3 in the YzRB (Fig. 6).

The national mean of simulated annual ET in China's landmass was 369.8 mm yr^{-1} from 2000 to 2010, which compares with global values reported in some previous studies. Dirmeyer et al. (2006) indicated that the global means of annual ET ranged from 272 to 441 mm yr^{-1} based on the simulations of 15 models in the Global Soil Wetness Project-2. However, mean ET in this study was lower than some recently reported global values. Fisher et al. (2008), using the Priestley–Taylor model and AVHRR remote sensing data, estimated that global mean ET equaled 444 mm yr^{-1} from 1986 to 1993, and Yuan et al. (2010) pointed out that

global mean ET was 417 ± 38 mm yr^{-1} across the vegetated area during the 2000–2003 period. Much higher global means of ET were also reported: 500 ± 104 mm yr^{-1} (Ryu et al., 2011), 539 ± 9 mm yr^{-1} (K. Zhang et al., 2010), 550 mm yr^{-1} (Jung et al., 2010), and 604 mm yr^{-1} (Zeng et al., 2012). In a synthesis study, Mueller et al. (2011) declared that the means of global ET ranged from 544 to 631 mm yr^{-1}, depending on which types of models were used. Therefore, it appears that the mean terrestrial ecosystems ET of China simulated here is somewhat lower than the global value (Fig. 5a).

The volumetric total ET over all terrestrial ecosystem areas in China varied from 3.26 to 3.65×10^3 km^3, the mean value being 3.49×10^3 km^3 from 2000 to 2010. This accounts to nearly 5 % of various reported global totals: 58.4×10^3 km^3 yr^{-1} (Yan et al., 2012), 63×10^3 km^3 yr^{-1} (Ryu et al., 2011), 65×10^3 km^3 yr^{-1} (Jung et al., 2010), 65.5×10^3 km^3 yr^{-1} (Oki and Kanae, 2006).
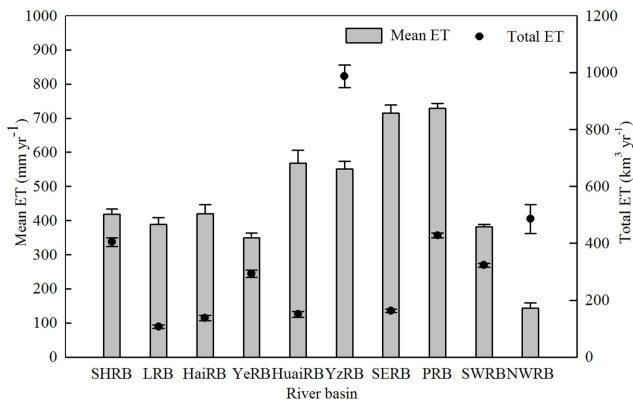
Fig. 6. The annual and total ET averaged over the period from 2000 to 2010 in 10 river basins: SHRB – Songhua River basin; LRB – Liaohe River basin; HaiRB – Haihe River basin; YeRB – Yellow River basin; HuaiRB – Huaihe River basin; YzRB – Yangtze River basin; SERB – southeast river basin; PRB – Pearl River basin; SWRB – southwest river basin; and NWRB – northwest river basin.

Fig. 7. Mean ET and total ET of different land cover types during the period from 2000 to 2010: ENF – evergreen needleleaf forest; EBF – evergreen broadleaf forest; DNF – deciduous needleleaf forest; DBF – deciduous broadleaf forest; MF – mixed forest; SHR – shrubland; GRA – grassland; CRO – cropland; NAV – cropland/natural vegetation mosaic; and NOV – non-vegetation.
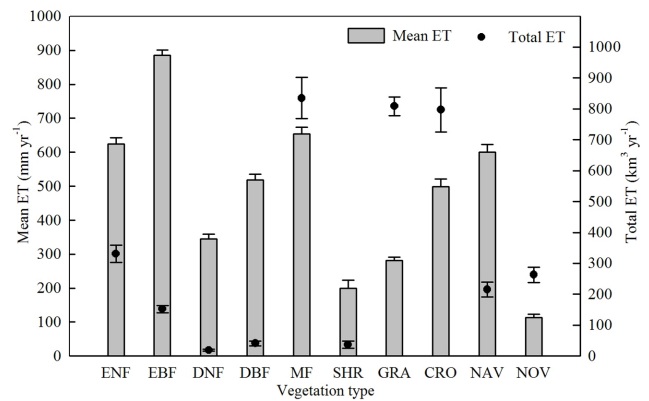
3.2.2 Spatial patterns of simulated annual water yield

Water yield showed a similar spatial pattern to ET, being above zero in most areas of China (Fig. 5b). However, in the arid NWRB there as insufficient precipitation to supply ET demand, resulting in slightly negative yield. In southern basins, precipitation was higher than ET, resulting in significantly positive water yield. For example, the yield was well above $600 \, \text{mm} \, \text{yr}^{-1}$ in the PRB and SERB, even above $1000 \, \text{mm} \, \text{yr}^{-1}$ in southeastern coastal areas. Yields in the vast YzRB ranged from $100 \, \text{mm} \, \text{yr}^{-1}$ in the upper basin to $800 \, \text{mm} \, \text{yr}^{-1}$ in the lower basin. Water yield was usually about $100 \, \text{mm} \, \text{yr}^{-1}$ in most regions of the SHRB, eastern LRB, HaiRB, and the upper basin of the YeRB.

3.2.3 Dependence of simulated ET on land cover types

Simulated ET from 2000 to 2010 is closely associated with land cover type (Fig. 7). The EBF biome has the largest average ET, $885.5 \, \text{mm} \, \text{yr}^{-1}$, followed by $653.3 \, \text{mm} \, \text{yr}^{-1}$ for MF and $624.0 \, \text{mm} \, \text{yr}^{-1}$ for ENF, the three much lower values being 345.4, 280.7, and $200.1 \, \text{mm} \, \text{yr}^{-1}$, respectively, for DNF, GRA, and SHR. The non-vegetation cover type, which is widely distributed in northwest China, has the lowest mean ET, amounting to $113.6 \, \text{mm} \, \text{yr}^{-1}$.

In terms of volumetric totals, the highest total annual ET, $834.70 \, \text{km}^3 \, \text{yr}^{-1}$, applies to MF, followed by the $808.60 \, \text{km}^3 \, \text{yr}^{-1}$ of GRA, and $796.27 \, \text{km}^3 \, \text{yr}^{-1}$ for CRO, the high totals being due to their large areas. Although the mean ET of EBF is the highest, the area total ET of this land cover type only ranked the seventh because of its relatively small area. Volumetric annual ET totals were less than $50 \, \text{km}^3 \, \text{yr}^{-1}$ for DNF, DBF, and SHR, owing to low mean ET per unit area or small land cover type areas of these.

The change of simulated ET with land cover type identified here is generally consistent with previous studies, which show that the ET of forest is higher than that of cropland and grassland (Liu et al., 2008; Zhou et al., 2009; K. Zhang et al., 2010; Jin et al., 2011; Li et al., 2012). However, the ET of ENF and MF simulated in this study is significantly higher than global values reported by K. Zhang et al. (2010). Recently, M. L. Liu et al. (2012) simulated an average ET over eastern China of $567 \, \text{mm} \, \text{yr}^{-1}$ between 2001 and 2005, about 10 % higher than the corresponding BEPS model value. Li et al. (2012) estimated a mean terrestrial ET of $\sim 505 \, \text{mm} \, \text{yr}^{-1}$ for China from 2000 to 2009, which is approximately 35 % higher than the estimate of this study.

3.3 Temporal trends in ET and water yield

3.3.1 Temporal trends in ET

ET increased in 62.2 % of China's landmass from 2000 to 2010 (Fig. 8). The greatest increase occurred in the cropland areas of the southern HaiRB, most of the HuaiRB, and the southeastern YzRB, with increases of more than $10 \, \text{mm} \, \text{yr}^{-1}$. Annual ET increased by 6 to $10 \, \text{mm} \, \text{yr}^{-1}$ in the northern HuaiRB and in forested areas of the western SHRB, YeRB and YzRB. The annual increases of ET were small in parts of the NWRB, only about $2 \, \text{mm} \, \text{yr}^{-1}$ in areas such as Inner Mongolia and Qinghai-Tibetan Plateau. On the other hand, annual ET decreased in the eastern SHRB, northwestern NWRB, southern SWRB and southern PRB. The ET decrease was most significant in the eastern Qinghai-Tibetan Plateau, the south part of Yunnan Province and in Hainan Province, the trend being $-8 \, \text{mm} \, \text{yr}^{-1}$.

Trends in the departures of simulated annual ET from 11 yr means in 10 basins show that annual ET increased in all
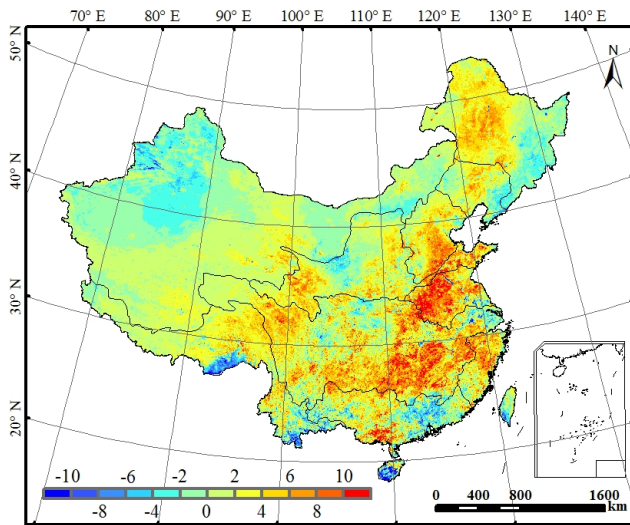
Fig. 8. Temporal trends of annual ET (mm yr^{-1}) in China from 2000 to 2010.

basins but the NWRB (Fig. 9). Increases of annual ET in the HuaiRB, YzRB and SWRB were above the 0.1 significance level. Annual ET in the YeRB, SHRB, SERB, HaiRB, PRB and LRB showed a relatively small increasing trend. In years from 2000 to 2002, especially in 2001, annual ET in all basins was lower than multi-year average values. In contrast, annual ET from 2004 to 2008 was mostly above multi-year averages in all basins. In 2009, ET decreased in all basins except the SERB, ET for the NWRB even decreasing by 15 % of the multi-year mean. Changes of ET relative to multi-year means varied spatially in 2003 and 2010, increases occurring in northern basins, decreases in southern basins.

The ET trends of the 2000–2010 period identified in southern China (Figs. 8 and 9) are consistent with the result reported by Jung et al. (2010) for 1998 to 2008. Both studies indicate decreasing trends of ET in the PRB and southern SERB, and increasing trends of ET in the YzRB and southern HuaiRB. Zeng et al. (2012) recently studied spatial-temporal changes of global land ET for the period from 1982 to 2009, using a land water mass balance equation, and found out that annual ET increased in the HuaiRB and HaiRB, but decreased in the PRB from 1998 to 2009. Similar temporal patterns of ET in these areas were also detected in this study for the period from 2000 to 2010. However, opposing ET trends between this study and another were found for the YzRB and SERB, Zeng et al. (2012) indicating that ET decreased in these two basins while this work detected increased ET.

National annual ET varied from 345.5 mm in 2001 to 387.8 mm in 2005, the average being 369.8 mm yr^{-1} from 2000 to 2010 (Fig. 10). ET exhibited a weak increasing trend across the terrestrial ecosystems of China during the study period, rising by 1.7 mm yr^{-1} ($R^2 = 0.18$, $p = 0.19$). National annual ET increased from 2001 to 2005, then gradually decreased to its second lowest value, 361.6 mm in 2009. In the

period from 2004 to 2008, the national land ET was above the multi-year average of 369.8 mm yr^{-1}. Decreases of ET in 2000, 2001, 2002 and 2009 were caused by the wide occurrence of severe droughts. Relatively low ET values were also found in 2000 and 2009 by Li et al. (2012). However, they reported a decreasing trend of ET for the 2003–2009 period.

3.3.2 Temporal trends in water yield

Temporal trends in water yield of terrestrial ecosystems from 2000 to 2010, exhibited substantial spatial heterogeneity (Fig. 11). Water yield decreased in northern, southern, southwestern and central China, but increased in northwestern, northeastern and eastern China. The water yield changed slightly in the NWRB and HaiRB, to the extent of ±4 mm yr^{-1}. Significant increases in water yield mainly occurred in the southeastern SHRB, eastern LRB and downstream areas of YzRB, with trends of close to 20 mm yr^{-1}. The YeRB experienced a moderate decrease in water yield, about 8 mm yr^{-1} during the 11 yr study period. Marked water yield decreases were found in the HuaiRB, SWRB, southern YzRB and western PRB, with trends stronger than -20 mm yr^{-1} in some areas.

Temporal trends of ET and water yield identified in this study imply that the terrestrial hydrological cycle intensified in most regions of China over recent 11 yr period, as indicated by significant ET increase in most areas, with consequent effects on the availability of water resources. In most regions south of the Yangtze River and the HuaiRB, enhanced ET in conjunction with decreased precipitation has caused water yield to decrease significantly. The temporal trends of ET and water yield in China identified here are consistent with previously reported on-going intensification of the global hydrological cycle over the 20th Century (Huntington, 2006; Wang et al., 2010; Yao et al., 2013).

3.4 Linkage of ET to climate factors

ET is affected by a variety of factors, including water availability, energy supply, wind speed, vapor pressure deficit (VPD) and vegetation activity (Zhang et al., 2001; Verstraeten et al., 2008; Wang and Dickinson, 2012). It is still a challenge to identify drivers for regional ET. In analyzing the roles of climate factors in ET, temperature is often used as the surrogate for radiation and VPD due to their strong correlations with temperature (Jung et al., 2010; Seneviratne et al., 2010; Zeng et al., 2012). Here annual precipitation was chosen as proxy for water availability, and mean annual temperature (MAT) as proxy for available energy, to explore the effects of climate variability on the spatial and temporal variations of ET over China's landmass from 2000 to 2010.

Over the study period, precipitation decreased significantly in southern China (Fig. 12a), in the HuaiRB, south YzRB, SWRB and PRB. In some parts of these regions,
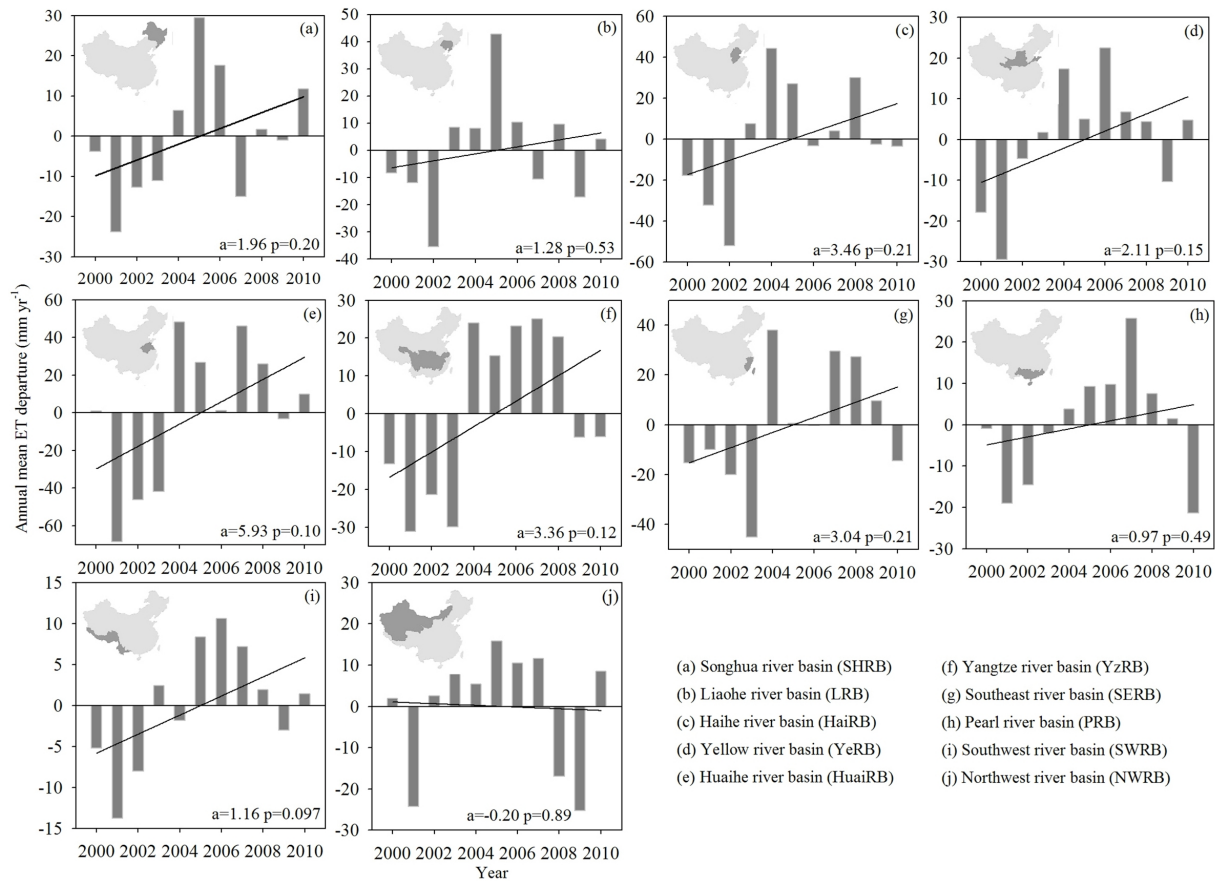
Fig. 9. Departures of annual ET from multi-year means in 10 basins from 2000 to 2010.
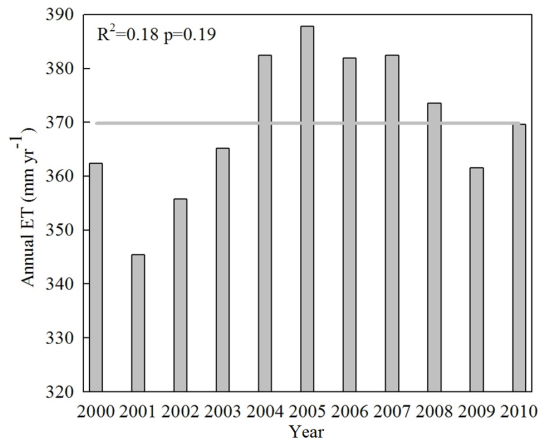
(a) Songhua river basin (SHRB) (f) Yangtze river basin (YzRB)
(b) Liaohe river basin (LRB) (g) Southeast river basin (SERB)
(c) Haihe river basin (HaiRB) (h) Pearl river basin (PRB)
(d) Yellow river basin (YeRB) (i) Southwest river basin (SWRB)
(e) Huaihe river basin (HuaiRB) (j) Northwest river basin (NWRB)

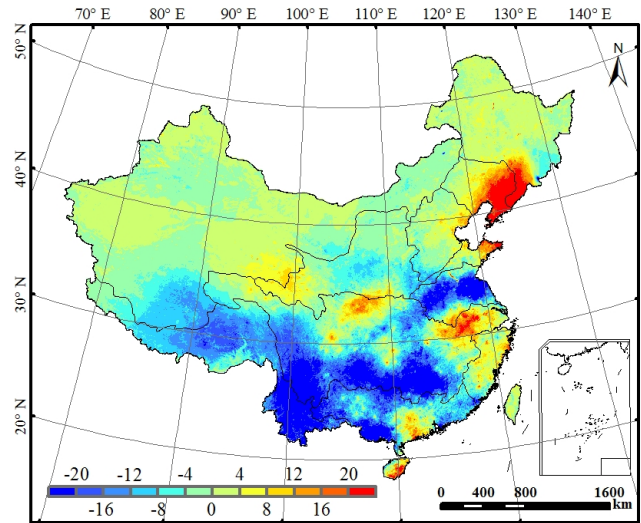**Fig. 10.** Interannual variations of annual ET averaged over China's landmass from 2000 to 2010.

Fig. 11. Temporal trends of water yield in China from 2000 to 2010 (mm yr^{-1}).

decreasing trends of annual precipitation were stronger than -24 mm yr^{-1}. Meanwhile, temperature increased by more than $0.04\,°C$ yr^{-1} (Fig. 12c), even more than $0.1\,°C$ yr^{-1} in the upper basin areas of the YzRB and SWRB. In northern China, MAT did not markedly increase while precipitation
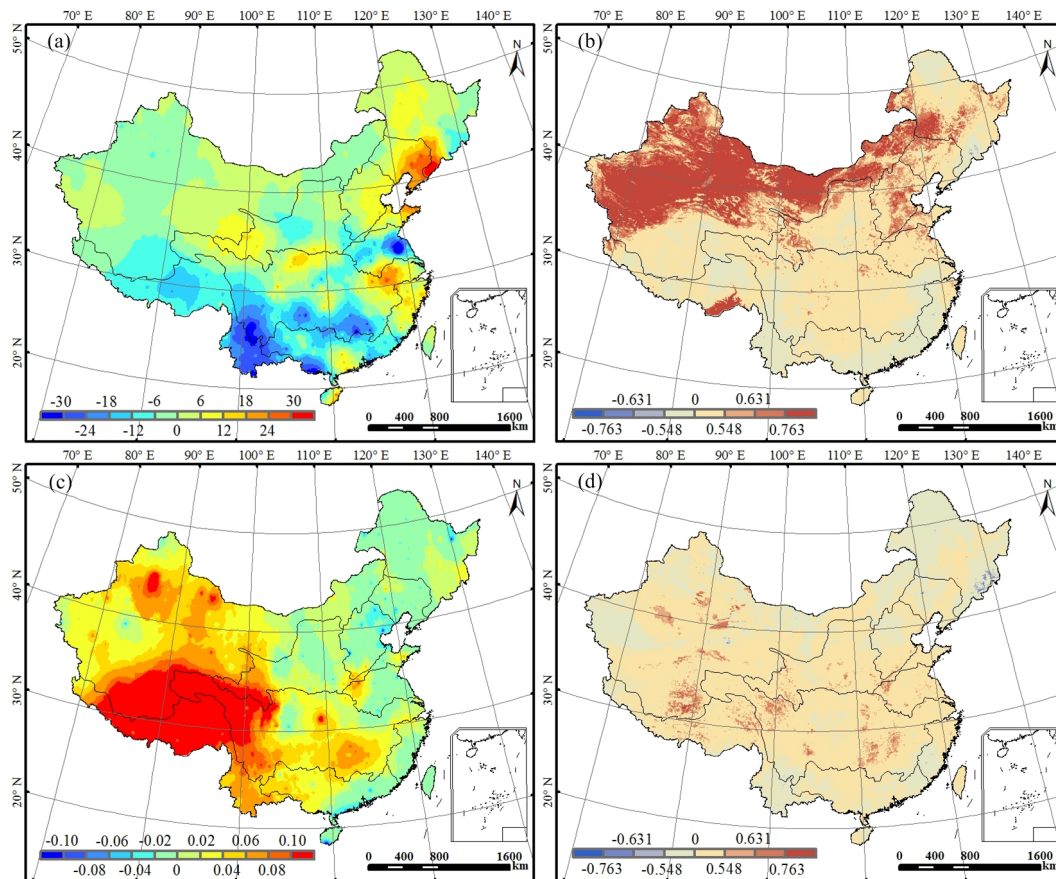
Fig. 12. Temporal trends of **(a)** annual precipitation (mm yr^{-1}) and **(c)** mean annual temperature (MAT) (°C yr^{-1}). Partial correlation coefficients for **(b)** annual precipitation and **(d)** MAT in relation to ET from 2000 to 2010. Partial correlation coefficients of 0.548, 0.631, and 0.763 indicate respective significance levels of 0.10, 0.05, and 0.01.

increased by 5–10 mm yr^{-1}. The decrease in precipitation and increase in temperature were induced by several severe drought events in southern China from 2000 to 2010 (Gao and Yang, 2009; Lu et al., 2011; Wang et al., 2011).

Figure 12b and d show the partial correlation coefficients of annual ET with annual total precipitation and MAT, respectively, during the period 2000–2010. Annual ET was positively correlated with annual precipitation in most regions of China (Fig. 12b), especially in the arid and semiarid regions of northern China, such as the NWRB, western SHRB, western LRB and HaiRB, in which there were significant positive correlations between ET and precipitation ($p < 0.01$). The marked increase of more than 8 mm yr^{-1} in annual ET in the HaiRB, western SHRB and upper basin of the YeRB (Fig. 8) is partially explained by the more than 6 mm yr^{-1} increase in annual precipitation in these regions. In humid southeastern China and the frigid Tibetan plateau, annual ET and precipitation were negatively correlated. In these regions, water supply is relatively sufficient, but precipitation increase is normally accompanied by reductions

in temperature and incoming solar radiation, with the consequent deceases of ET.

Annual ET increased with MAT increase in the Qinghai-Tibetan Plateau, the PRB, some areas of the NWRB, most of the YzRB and YeRB, and in the HuaiRB (Fig. 12d). In the Qinghai-Tibetan Plateau, especially the southeastern part of the NWRB, most of the SWRB, and upper basin areas of the YeRB and YzRB, positive correlations of ET with MAT were above the 0.1 significant level. Temperature acts as the major limiting factor of ET in these regions. The increase of nearly 0.1 °C yr^{-1} here (Fig. 12c) was the main driver of a more than 4 mm yr^{-1} trend in annual ET (Fig. 8). Alternatively, in the western NWRB, most of the SHRB, LRB, and the southern SERB, annual ET was negatively correlated with MAT.

Departures of annual ET from multi-year means were plotted with the departures of annual total precipitation and MAT from their multi-year means for individual basins to see if change in ET could be associated with changes in one or both of the other two (Fig. 13). ET departures showed much stronger dependencies on precipitation departures in northern than in southern basins, notably the SHRB, LRB, HaiRB,
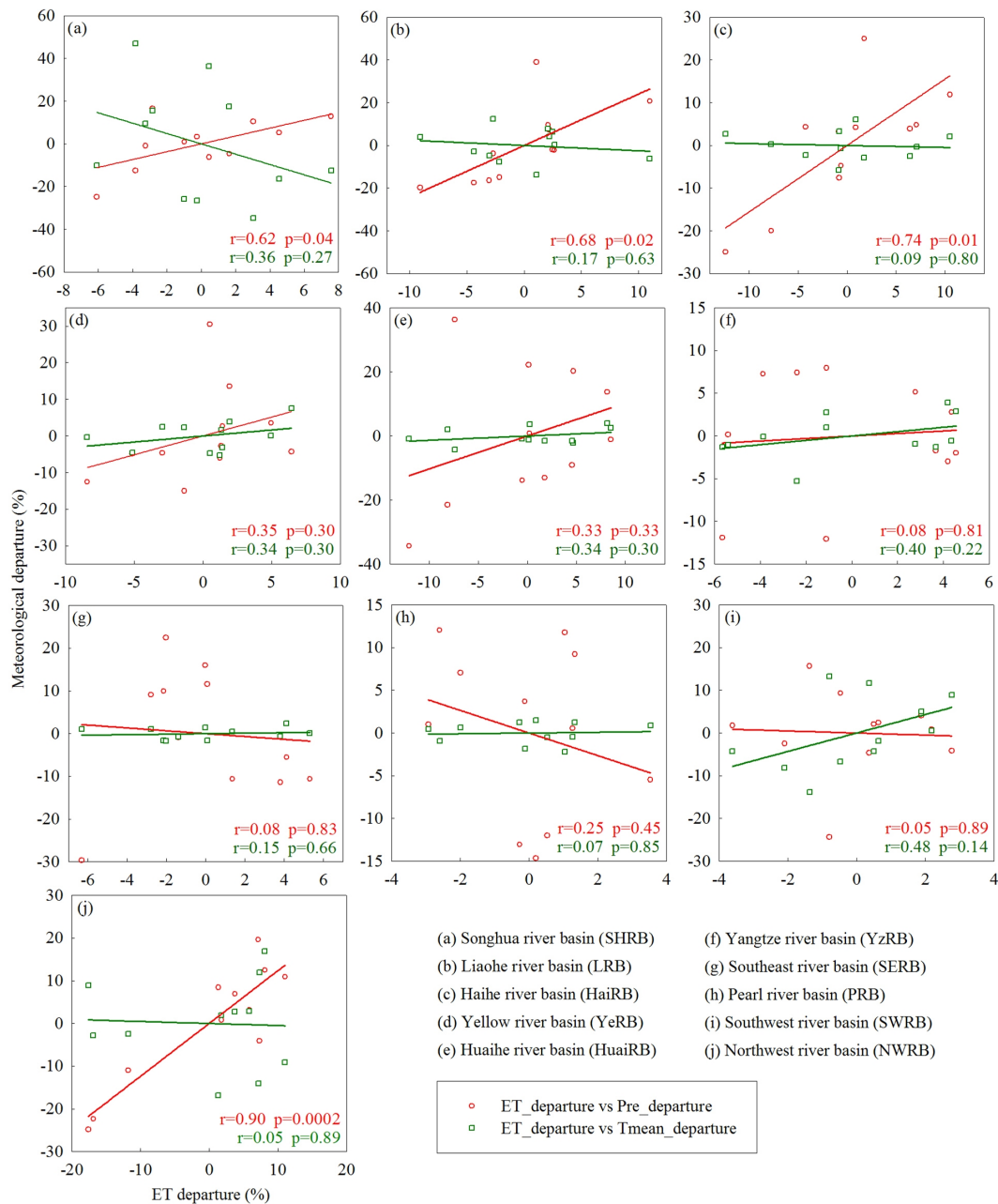
Fig. 13. Correlations of the departures of basin-level annual ET with the departures of precipitation and temperature.

YeRB and NWRB, where departures of annual ET were positively correlated with those of precipitation. The correlations were above the 0.05 significance level in the SHRB and LRB, and above the 0.01 significance level in the HaiRB and NWRB. Changes in precipitation did not have significant impact on ET in the humid southern regions of China; in fact, their respective departures were slightly negatively correlated in the SERB, PRB and SWRB. Basin-level ET change was not significantly correlated with MAT departures in any of the basins.

Several previous studies have investigated the controlling roles of different climate factors in ET from terrestrial ecosystems in China. Zhou et al. (2009) pointed out that precipitation plays a more important role in altering the inter-annual variations of annual ET over China than temperature does. Cong et al. (2010) concluded that precipitation had a greater impact on ET in the north than in the south. In a study on global ET linkages to MAT and precipitation during the 1982–2008 period, Jung et al. (2010) declared that precipitation dominated inter-annual ET behavior in northern China, but in southern China ET was mainly temperature limited.
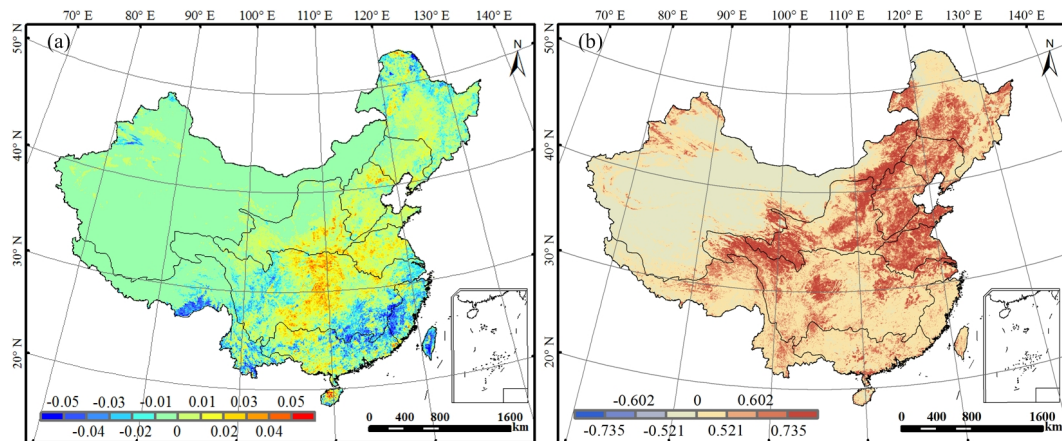
Fig. 14. (a) Temporal trends of LAI and **(b)** the correlation coefficients of annual LAI with annual ET from 2000 to 2010. Correlation coefficients of 0.521, 0.602, and 0.735 indicate respective significance levels of 0.10, 0.05, and 0.01.

ET in the semi-arid and arid northern areas of China was limited by the supply of soil moisture, which is significantly affected by precipitation, the key constraining factor of ET here (Ryu et al., 2008; Wang and Dickinson, 2012). Using daily meteorological data and gauging station data, Zhang et al. (2011b) indicated that precipitation was the major determinant of ET in the YeRB. Xiao et al. (2013) recently synthesized observations from 22 eddy-covariance flux sites across China and found that the northern ecosystems had high annual ET largely because of the high temperature and abundant water supply, while semiarid, subalpine and alpine ecosystems had relatively low ET mainly because of low precipitation and lower temperatures, respectively. The effects of temperature and precipitation on ET identified here are generally similar to previous findings, but with more detail due to the higher spatial resolution of simulation and application of remote sensing data.

3.5 Vegetation influences on ET

3.5.1 Changes of ET with LAI

LAI significantly affects ET due to its roles in transpiration and interception of precipitation. During the period 2000–2010, annual LAI increased in northeastern, northern and most south central China, while it decreased in southeastern and parts of southwestern China (Fig. 14a) due to climatic abnormality and land cover changes (Peng et al., 2011; Y. Liu et al., 2012). Similar conclusions on vegetation greenness in China during the same period were recently reported by Liu and Gong (2012).

Simulated annual ET over the study period was found to be positively correlated with annual LAI in 74 % of China's landmass (Fig. 14b). The correlation between LAI and ET was stronger in the north than in the south. In most of the SHRB, LRB, HaiRB, HuaiRB and YeRB, as well as part of the YzRB, annual ET increased significantly ($p < 0.05$) with

LAI increase. Thus, the trend of more than $8\,\mathrm{mm\,yr^{-1}}$ annual ET increase in the HaiRB, HuaiRB, and central YzRB can be partially explained by the significant increase in annual LAI here ($> 0.03\,\mathrm{yr^{-1}}$). Annual ET was slightly positively correlated with annual LAI in most regions south of the Yangtze River, such as the SERB, southern YzRB and PRB. The distinguishable annual ET decrease for southern China, in areas such as the southern Qinghai-Tibetan Plateau, the junction area of the YzRB, SWRB and PRB, and eastern PRB might be caused by the significant decrease in annual LAI found here. In most of the NWRB, vegetation cover is relatively low and thus evaporation from soil is the dominant ET component. An increase in LAI might cause transpiration to increase, thus decreasing in soil evaporation. As a consequence, the correlation of ET with LAI was slightly negative here.

3.5.2 Influences of land cover change on ET

ET is closely linked with land cover types. Model simulation and site observations showed that the ET of forests was generally higher than that of croplands and grasslands (Zhang et al., 2001; Liu et al., 2008; Mu et al., 2011). Land cover changes have been dynamically occurring in China, driven by afforestation, reforestation and urbanization, inevitably leading to increases in plantations and urban areas, and decreases in croplands and grasslands areas (Li et al., 2011; Wang et al., 2012). In order to assess the effects of land cover changes on regional ET, the mean of ET, and changing rates of mean ET, total ET, areas of the various forest cover types (including ENF, EBF, DNF, DBF, and MF), cropland, and grassland were calculated for 10 basins (Table 4).

The national annual ET of forests, cropland, and grassland increased during the study period (Table 4). The annual ET of cropland showed that the largest increase trend, $2.38\,\mathrm{mm\,yr^{-1}}$, followed by those of forest and grassland. As for forest, the annual ET increased in most basins except

Table 4. Trends in ET and areas of forest, cropland, and grassland in 10 basins from 2000 to 2010.

	Mean ET (mm yr⁻¹)				Trend of mean ET (mm yr⁻¹)				Trend of total ET (km³ yr⁻¹)				Trend of total area (10⁶ ha yr⁻¹)		
	All land covers	Forest	Cropland	Grassland	All land covers	Forest	Cropland	Grassland	All land covers	Forest	Cropland	Grassland	Forest	Cropland	Grassland
SHRB	418.9	465.7	410.1	343.3	1.96	0.95	1.95	2.28	1.90	1.52^b	−0.04	0.17	0.27^b	−0.28	−0.02
LRB	389.2	539.0	409.9	344.6	1.28	−3.74	1.62	2.32	0.35	0.29^b	−0.41	0.53	0.066^c	−0.21^b	0.12^a
HaiRB	419.4	483.9	444.0	395.1	3.46	2.60	4.17	2.71	0.34^b	0.34^b	0.97	0.13	0.09^b	−0.05	0.02
YeRB	349.0	532.7	431.6	315.2	2.11	2.31	1.55	1.46	1.77	0.49^c	−0.05	−0.05	0.10^b	0.22	−0.26^b
HuaiRB	568.1	638.7	586.2	559.9	5.93^a	5.50	6.70*	−1.79	1.58^a	0.30^c	1.85^a	−0.43^c	0.04^c	0.02	−0.06^b
YzRB	551.7	652.0	604.9	327.7	3.36	4.24	2.60	−0.30	6.01	9.71^c	−0.59	−1.01	1.11^c	−0.58	−0.28^c
SERB	714.4	771.1	615.9	637.5	3.04	3.43	−0.94	−4.83	0.69	0.90^b	0.09	−0.05	0.05^a	−0.007	−0.002
PRB	729.3	770.5	656.2	677.7	0.97	0.45	−3.37^a	−9.76^c	0.57	−0.21	−0.43	−0.80^c	−0.03	−0.12	−0.08^b
SWRB	381.6	707.4	554.9	246.2	1.16^a	−0.94	−1.0	1.22	0.99^a	0	−0.18^b	0.99^b	0.06	−0.04^b	0.11
NWRB	143.9	234.3	225.2	200.2	−0.20	−1.15	−3.19	−0.31	−0.69	0.02	−0.10	1.76	0.03	0.05	1.0^c
Total	369.8	651.4	498.3	280.7	1.71	1.64	2.38	0.42	14.29	13.35^c	2.83	1.25	1.79^c	−0.99	0.55

Note: ^{a}, ^{b}, and ^{c} represent the 0.10, 0.05, and 0.01 significance levels, respectively (SHRB, Songhua River basin; LRB, Liaohe River basin; HaiRB, Haihe River basin; YeRB, Yellow River basin; HuaiRB, Huaihe River basin; YzRB, Yangtze River basin; SERB, southeast river basin; PRB, Pearl River basin; SWRB, southwest river basin; NWRB, northwest river basin).
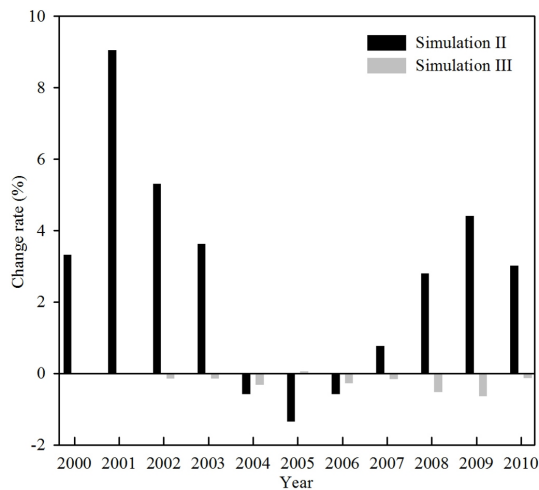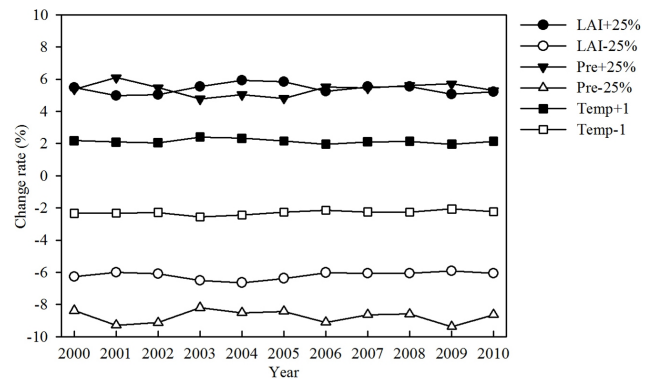
Fig. 15. Changes in national total ET output from Simulations II and III relative to that simulated in Simulation I.

Fig. 16. Changes of simulated national total ET under different disturbance scenarios of precipitation, temperature, and LAI relative to the corresponding values simulated using undisturbed inputs during the 2000–2010 period.

the LRB, SWRB and NWRB. The annual ET of cropland and grassland increased in northern and decreased in southern basins. In the PRB, the annual ET values of cropland and grassland decreased at rates of 3.37 ($p < 0.1$) and 9.76 mm yr^{-1} ($p < 0.01$), respectively.

The national volumetric total ET values of forest, cropland and grassland all increased during the 2000–2010 period. The total ET of forests increased significantly in seven basins, causing the national total ET of forests to increase at a rate of 13.35 km^3 yr^{-1} ($p < 0.01$). The increase in national total ET of forests was driven by increases in both annual ET amounts and areas, but the expansion of forest area played a more dominant role. During the past 11 yr, the national total of forest area increased at a rate of 1.79×10^6 ha yr^{-1} ($p < 0.01$). The national total ET of cropland increased at a rate of 2.83 km^3 yr^{-1}, mainly driven by increases in annual ET, because total cropland area decreased at a rate of 0.99×10^6 ha yr^{-1}. The total ET of cropland increased in the HaiRB, YeRB, HuaiRB and SERB, but decreased in other six basins. The national total ET of grassland increased by 1.25 km^3 yr^{-1}, driven by increases in both annual ET and area. Total ET amounts for grassland increased in most northern and decreased in most southern basins except for the SWRB. The decrease in total ET from grassland in southern basins was caused by decreases in both annual ET and area. In the HuaiRB and PRB, total ET amounts from grassland significantly decreased, at rates of 0.43 and 0.80 km^3 yr^{-1} ($p < 0.01$) for each respective basin.

During the 2000–2010 period, total ET from China's terrestrial ecosystems increased at a rate of 14.29 km^3 yr^{-1}. This might mainly be attributed to the total ET increasing trend of 13.35 km^3 yr^{-1} for forests. The simulations showed that ET estimates from forests were higher than for other land cover types (Fig. 7), similar to the findings of previous studies, which reported that conversion from crop and

grass to forest can cause annual ET to increase and water yield to decrease (Twine et al., 2004; Sun et al., 2005, 2006; Yu et al., 2009; Zhang et al., 2011b). Sun et al. (2006) indicated that the average water yield reduction caused by land cover conversion varied from ~ 50 mm yr^{-1} (50 % of initial) in the semiarid Loess Plateau region of northern China to ~ 300 mm yr^{-1} (30 % of initial) in the tropical southern region. According to hydrological model simulations, Yu et al. (2009) declared that changing grassland into forest caused a significant reduction of water yield and an increase of ET in a watershed of the Liupan Mountains, northwest China. Based on daily meteorological and gauging stations data, Zhang et al. (2011b) found that intensifying urbanization acted towards decreasing ET in the PRB.

Figure 15 shows changes of the national ET output from Simulations II and III in comparison with the value from Simulation I. The national annual ET in Simulation II (no climate variability) was obviously larger than the corresponding values of Simulation I, especially in the years of 2001, 2002 and 2009, implying climate variability had a negative effect on ET. In contrast, the national total ET simulated in Simulation III was smaller than the corresponding values output from Simulation I, indicating that land cover change enhanced ET during the 2000–2010 period.

Simulated ET is sensitive to model inputs, which might have some uncertainties. Additional simulations were conducted to assess the impacts of uncertainties in temperature, precipitation, and LAI on simulated national total ET. In each simulation, one input was disturbed by a certain magnitude for all pixels while all other variables remained undisturbed. Figure 16 shows the relative changes of national total national ET during the 2000–2010 period. The national annual ET would increase or decrease by about 6 % while LAI increased or decreased by 25 %. Simulated ET was more sensitive to precipitation than to temperature. National mean annual ET would change about 2 % when the temperature

changed by $\pm 1\,^\circ$C. If precipitation decreased or increased by 25 %, simulated national total ET would decrease by more than 8 % or increase by about 5–6 %. The effects of precipitation change on ET were particularly obvious in the drought years and water limited regions.

4 Conclusions

The BEPS model was employed in conjunction with the newly developed data set of LAI to simulate ET and water yield in China at a spatial resolution of 500 m, from 2000 to 2010. The ability of BEPS to simulate ET was first validated using tower-based ET at five ChinaFLUX sites. Then the spatial and temporal variations of ET, water yield, and the influences of climatic and vegetation factors were analyzed. The following conclusions are drawn:

1. The BEPS model is able to simulate ET in China's terrestrial ecosystems, explaining 66 % of the variations of observed daily ET at five ChinaFLUX sites. The RPE values of simulated annual ET are mostly within ± 10 % of the observed values.

2. Simulated annual ET exhibited a distinguishable decreasing spatial pattern from southeast to northwest, in association with climate and vegetation types. Annual ET increased with increasing LAI in 74 % of China's landmass, especially in the SHRB, LRB, HaiRB, HuaiRB and YeRB. It was positively correlated with temperature in the southeastern part of the NWRB, most of the SWRB, and upper basin areas of the YeRB and YzRB. In the arid and semiarid areas of northwest and north China, annual ET was significantly positively correlated with annual precipitation, while the correlation between precipitation and ET was negative in the Tibetan Plateau and humid southeast China.

3. The national annual ET averaged 369.8 mm yr^{-1} during the 2000–2010 period, ranging from 345.5 mm in 2001 to 387.8 mm in 2005. It increased at a rate of 1.7 mm yr^{-1} ($R^2 = 0.18$, $p = 0.19$), mainly driven by an increase of ET in forests. National total ET increased during the period from 2001 to 2005, and decreased during the period from 2006 to 2009. Climate variability had a larger effect on the trend of simulated national ET than land cover change. Simulated national total ET was more sensitive to precipitation than to LAI and temperature.

4. In 62.2 % of China's terrestrial ecosystems, ET showed increasing trends, especially in the cropland areas of the southern HaiRB, most of the HuaiRB and the southeastern YzRB. The decrease of annual ET mainly occurred in some areas of northeast, north, northwest, south China. In eastern Qinghai-Tibetan Plateau, the south of Yunnan Province and Hainan

Province, the decrease in ET was most significant, stronger than -8 mm yr^{-1}.

5. Water yield was above zero in most China's terrestrial ecosystems, especially in southeast and south regions. However, it was negative in most areas of NWRB in northwest China. Water yield decreased in northern, southern, and southwestern China during the studied period. In some areas, water yield even decreased at rates more than 20 mm yr^{-1} because of enhanced ET and precipitation decrease. This implies that climatic variability and vegetation changes have significantly intensified terrestrial hydrological cycle and reduced water resource in these areas. Regions with water yield increase were sporadically distributed in northeast, east, south, northwest and central China, where increase may be due to precipitation increase, ET decreased, or both.

This study investigates the variations of ET and water yield over 11 recent years in China. It offers new insights for managing water resources efficiently and, because of the interactions of the water and carbon cycles and the strengths of the BEPS model in representing these, provides future opportunities for studying the carbon cycle in China. However, it should be kept in mind that there are still some uncertainties. In this study, we focused on national/regional and interannual variations of ET and water yield. The seasonal variation and more detailed spatial analysis (building from the 500 m grid) could be further explored in the future. Although most spatial data sets driving the model were taken from ground observations and remote sensing data, some uncertainties may exist in the data sets, such as limited meteorological observations and errors in remotely sensed vegetation parameters. Model validation was only done at a few sites. In addition, shortcomings in the structure of the BEPS model, such as the exclusion of irrigation and lateral movement from soil water content calculation, might cause some errors in estimated ET and water yield. All such deficiencies need to be addressed in future research.

Edited by: G. Jewitt

References

Amthor, J. S., Chen, J. M., Clein, J. S., Frolking, S. E., Goulden, M. L., Grant, R. F., Kimball, J. S., King, A. W., McGuire, A. D., Nikolov, N. T., Potter, C. S., Wang, S., and Wofsy, S. C.: Boreal forest CO_2 exchange and evapotranspiration predicted by nine ecosystem process models: Intermodel comparisons and relationships to field measurements, J. Geophys. Res.-Atmos., 106, 33623–33648, doi:10.1029/2000jd900850, 2001.

Anderson, R. G., Jin, Y., and Goulden, M. L.: Assessing regional evapotranspiration and water balance across a Mediterranean montane climate gradient, Agr. Forest Meteorol., 166–167, 10–22, doi:10.1016/j.agrformet.2012.07.004, 2012.

Bunce, J.: Carbon dioxide effects on stomatal responses to the environment and water use by crops under field conditions, Oecologia, 140, 1–10, doi:10.1007/s00442-003-1401-6, 2004.

Cao, S. X., Chen, L., Shankman, D., Wang, C. M., Wang, X. B., and Zhang, H.: Excessive reliance on afforestation in China's arid and semi-arid regions: Lessons in ecological restoration, Earth-Sci Rev., 104, 240–245, doi:10.1016/j.earscirev.2010.11.002, 2011.

Chen, B. Z., Chen, J. M., and Ju, W. M.: Remote sensing-based ecosystem-atmosphere simulation scheme (EASS) – Model formulation and test with multiple-year data, Ecol. Model., 209, 277–300, 2007.

Chen, J. M. and Leblanc, S. G.: A four-scale bidirectional reflectance model based on canopy architecture, IEEE T. Geosci. Remote, 35, 1316–1337, 1997.

Chen, J. M., Liu, J., Cihlar, J., and Goulden, M. L.: Daily canopy photosynthesis model through temporal and spatial scaling for remote sensing applications, Ecol. Model., 124, 99–119, 1999.

Chen, J. M., Chen, X. Y., Ju, W. M., and Geng, X. Y.: Distributed hydrological model for mapping evapotranspiration using remote sensing inputs, J. Hydrol., 305, 15–39, 2005.

Chen, J. M., Deng, F., and Chen, M. Z.: Locally adjusted cubic-spline capping for reconstructing seasonal trajectories of a satellite-derived surface parameter, IEEE T. Geosci. Remote, 44, 2230–2238, 2006.

Chen, J. M., Mo, G., Pisek, J., Liu, J., Deng, F., Ishizawa, M., and Chan, D.: Effects of foliage clumping on the estimation of global terrestrial gross primary productivity, Global Biogeochem. Cy., 26, GB1019, doi:10.1029/2010gb003996, 2012.

Cheng, L., Xu, Z., Wang, D., and Cai, X.: Assessing interannual variability of evapotranspiration at the catchment scale using satellite-based evapotranspiration data sets, Water Resour. Res., 47, W09509, doi:10.1029/2011wr010636, 2011.

Cong, Z. T., Zhao, J. J., Yang, D. W., and Ni, G. H.: Understanding the hydrological trends of river basins in China, J. Hydrol., 388, 350–356, doi:10.1016/j.jhydrol.2010.05.013, 2010.

Courault, D., Seguin, B., and Olioso, A.: Review on estimation of evapotranspiration from remote sensing data: From empirical to numerical modeling approaches, Irrig. Drain. Syst., 19, 223–249, doi:10.1007/s10795-005-5186-0, 2005.

Deng, F., Chen, J. M., Plummer, S., Chen, M. Z., and Pisek, J.: Algorithm for global leaf area index retrieval using satellite imagery, IEEE T. Geosci. Remote, 44, 2219–2229, doi:10.1109/tgrs.2006.872100, 2006.

Dirmeyer, P. A., Gao, X., Zhao, M., Guo, Z., Oki, T., and Hanasaki, N.: GSWP-2: Multimodel analysis and implications for our perception of the land surface, B. Am. Meteorol. Soc., 87, 1381–1397, doi:10.1175/bams-87-10-1381, 2006.

El Maayar, M. and Chen, J. M.: Spatial scaling of evapotranspiration as affected by heterogeneities in vegetation, topography, and soil texture, Remote Sens. Environ., 102, 33–51, 2006.

Fang, J., Tang, Y., and Son, Y.: Why are East Asian ecosystems important for carbon cycle research?, Sci. China Life Sci., 53, 753–756, doi:10.1007/s11427-010-4032-2, 2010.

FAO: Food and Agriculture Organization: Global Forest Resources Assessment, Rome, Italy, 2010.

Farquhar, G. D., Caemmerer, S. V., and Berry, J. A.: A biochemical-model of photosynthetic CO_2 assimilation in leaves of C_3 species, Planta, 149, 78–90, 1980.

Feng, X., Liu, G., Chen, J. M., Chen, M., Liu, J., Ju, W. M., Sun, R., and Zhou, W.: Net primary productivity of China's terrestrial ecosystems from a process model driven by remote sensing, J. Environ. Manage., 85, 563–573, doi:10.1016/j.jenvman.2006.09.021, 2007.

Fernández-Prieto, D., van Oevelen, P., Su, Z., and Wagner, W.: Editorial "Advances in Earth observation for water cycle science", Hydrol. Earth Syst. Sci., 16, 543–549, doi:10.5194/hess-16-543-2012, 2012.

Fisher, J. B., Tu, K. P., and Baldocchi, D. D.: Global estimates of the land-atmosphere water flux based on monthly AVHRR and ISLSCP-II data, validated at 16 FLUXNET sites, Remote Sens. Environ., 112, 901–919, 2008.

Fisher, J. B., Whittaker, R. J., and Malhi, Y.: ET come home: potential evapotranspiration in geographical ecology, Global Ecol. Biogeogr., 20, 1–18, doi:10.1111/j.1466-8238.2010.00578.x, 2011.

Friedl, M. A., McIver, D. K., Hodges, J. C. F., Zhang, X. Y., Muchoney, D., Strahler, A. H., Woodcock, C. E., Gopal, S., Schneider, A., Cooper, A., Baccini, A., Gao, F., and Schaaf, C.: Global land cover mapping from MODIS: algorithms and early results, Remote Sens. Environ., 83, 287–302, doi:10.1016/s0034-4257(02)00078-0, 2002.

Friedl, M. A., Sulla-Menashe, D., Tan, B., Schneider, A., Ramankutty, N., Sibley, A., and Huang, X.: MODIS Collection 5 global land cover: Algorithm refinements and characterization of new datasets, Remote Sens. Environ., 114, 168–182, doi:10.1016/j.rse.2009.08.016, 2010.

Gao, G., Chen, D., Xu, C.-Y., and Simelton, E.: Trend of estimated actual evapotranspiration over China during 1960–2002, J. Geophys. Res.-Atmos., 112, D11120, doi:10.1029/2006jd008010, 2007.

Gao, H., and Yang, S.: A severe drought event in northern China in winter 2008-2009 and the possible influences of La Nina and Tibetan Plateau, J. Geophys. Res.-Atmos., 114, D24104, doi:10.1029/2009JD012430, 2009.

Govind, A., Chen, J. M., and Ju, W. M.: Spatially explicit simulation of hydrologically controlled carbon and nitrogen cycles and associated feedback mechanisms in a boreal ecosystem, J. Geophys. Res.-Biogeo., 114, G02006, doi:10.1029/2008JG000728, 2009a.

Govind, A., Chen, J. M., Margolis, H., Ju, W. M., Sonnentag, O., and Giasson, M. A.: A spatially explicit hydro-ecological modeling framework (BEPS-TerrainLab V2.0): Model description and test in a boreal ecosystem in Eastern North America, J. Hydrol., 367, 200–216, doi:10.1016/j.jhydrol.2009.01.006, 2009b.

Gowda, P. H., Chavez, J. L., Colaizzi, P. D., Evett, S. R., Howell, T. A., and Tolk, J. A.: Remote sensing based energy balance algorithms for mapping ET: Current status and future challenges, T. ASABE, 50, 1639–1644, 2007.

Grant, R. F., Arain, A., Arora, V., Barr, A., Black, T. A., Chen, J., Wang, S., Yuan, F., and Zhang, Y.: Intercomparison of techniques to model high temperature effects on CO_2 and energy exchange in temperate and boreal coniferous forests, Ecol. Model., 188, 217–252, doi:10.1016/j.ecolmodel.2005.01.060, 2005.

Grant, R. F., Zhang, Y., Yuan, F., Wang, S., Hanson, P. J., Gaumont-Guay, D., Chen, J., Black, T. A., Barr, A., Baldocchi, D. D., and Arain, A.: Intercomparison of techniques to model water stress effects on CO_2 and energy exchange in temperate and boreal deciduous forests, Ecol. Model., 196, 289–312, doi:10.1016/j.ecolmodel.2006.02.015, 2006.

Huang, L., Liu, J., Shao, Q., and Xu, X.: Carbon sequestration by forestation across China: Past, present, and future, Renew. Sust. Energ. Rev., 16, 1291–1299, doi:10.1016/j.rser.2011.10.004, 2012.

Huntington, T. G.: Evidence for intensification of the global water cycle: Review and synthesis, J. Hydrol., 319, 83–95, 2006.

Hutjes, R. W. A., Kabat, P., Running, S. W., Shuttleworth, W. J., Field, C., Bass, B., Dias, M., Avissar, R., Becker, A., Claussen, M., Dolman, A. J., Feddes, R. A., Fosberg, M., Fukushima, Y., Gash, J. H. C., Guenni, L., Hoff, H., Jarvis, P. G., Kayane, I., Krenke, A. N., Liu, C., Meybeck, M., Nobre, C. A., Oyebande, L., Pitman, A., Pielke, R. A., Raupach, M., Saugier, B., Schulze, E. D., Sellers, P. J., Tenhunen, J. D., Valentini, R., Victoria, R. L., and Vorosmarty, C. J.: Biospheric aspects of the hydrological cycle - Preface, J. Hydrol., 212, 1–21, doi:10.1016/s0022-1694(98)00255-8, 1998.

Jarvis, P. G.: The interpretation of variations in leaf water potential and stomatal conductance found in canopies in field, Philos. T. Roy. Soc. B, 273, 593–610, 1976.

Jia, Z., Liu, S., Xu, Z., Chen, Y., and Zhu, M.: Validation of remotely sensed evapotranspiration over the Hai River Basin, China, J. Geophys. Res.-Atmos., 117, D13113, doi:10.1029/2011jd017037, 2012.

Jiang, L. and Islam, S.: A methodology for estimation of surface evapotranspiration over large areas using remote sensing observations, Geophys. Res. Lett., 26, 2773–2776, doi:10.1029/1999gl006049, 1999.

Jin, Y., Randerson, J. T., and Goulden, M. L.: Continental-scale net radiation and evapotranspiration estimated using MODIS satellite observations, Remote Sens. Environ., 115, 2302–2319, doi:10.1016/j.rse.2011.04.031, 2011.

Ju, W. M., Chen, J. M., Black, T. A., Barr, A. G., Liu, J., and Chen, B. Z.: Modelling multi-year coupled carbon and water fluxes in a boreal aspen forest, Agr. Forest Meteorol., 140, 136–151, 2006.

Ju, W. M., Gao, P., Wang, J., Zhou, Y. L., and Zhang, X. H.: Combining an ecological model with remote sensing and GIS techniques to monitor soil water content of croplands with a monsoon climate, Agr. Water Manage., 97, 1221–1231, 2010.

Jung, M., Reichstein, M., Ciais, P., Seneviratne, S. I., Sheffield, J., Goulden, M. L., Bonan, G., Cescatti, A., Chen, J., de Jeu, R., Dolman, A. J., Eugster, W., Gerten, D., Gianelle, D., Gobron, N., Heinke, J., Kimball, J., Law, B. E., Montagnani, L., Mu, Q., Mueller, B., Oleson, K., Papale, D., Richardson, A. D., Roupsard, O., Running, S., Tomelleri, E.,

Viovy, N., Weber, U., Williams, C., Wood, E., Zaehle, S., and Zhang, K.: Recent decline in the global land evapotranspiration trend due to limited moisture supply, Nature, 467, 951–954, doi:10.1038/nature09396, 2010.

Kelliher, F. M., Leuning, R., Raupach, M. R., and Schulze, E. D.: Maximum conductances for evaporation from global vegetation types, Agr. Forest Meteorol., 73, 1–16, doi:10.1016/0168-1923(94)02178-m, 1995.

Koster, R. D., Dirmeyer, P. A., Guo, Z. C., Bonan, G., Chan, E., Cox, P., Gordon, C. T., Kanae, S., Kowalczyk, E., Lawrence, D., Liu, P., Lu, C. H., Malyshev, S., McAvaney, B., Mitchell, K., Mocko, D., Oki, T., Oleson, K., Pitman, A., Sud, Y. C., Taylor, C. M., Verseghy, D., Vasic, R., Xue, Y. K., Yamada, T., and Team, G.: Regions of strong coupling between soil moisture and precipitation, Science, 305, 1138–1140, 2004.

Li, J., Yu, Q., Sun, X., Tong, X., Ren, C., Wang, J., Liu, E., Zhu, Z., and Yu, G.: Carbon dioxide exchange and the mechanism of environmental control in a farmland ecosystem in North China Plain, Sci. China Ser. D, 49, 226–240, doi:10.1007/s11430-006-8226-1, 2006.

Li, X., Ju, W., Zhou, Y., and Chen, S.: Retrieving leaf area index of forests in red soil hilly region using remote sensing data, Second International Conference on Earth Observation for Global Changes (EOGC 2009): Remote Sensing of Earth Surface Changes, Chengdu, China, 74710–74719, 2009.

Li, X., Liang, S., Yuan, W., Yu, G., Cheng, X., Chen, Y., Zhao, T., Feng, J., Ma, Z., Ma, M., Liu, S., Chen, J., Shao, C., Li, S., Zhang, X., Zhang, Z., Sun, G., Chen, S., Ohta, T., Varlagin, A., Miyata, A., Takagi, K., Saiqusa, N., and Kato, T.: Estimation of evapotranspiration over the terrestrial ecosystems in China, Ecohydrology, doi:10.1002/eco.1341, in press, 2012.

Li, Z., Yu, G., Xiao, X., Li, Y., Zhao, X., Ren, C., Zhang, L., and Fu, Y.: Modeling gross primary production of alpine ecosystems in the Tibetan Plateau using MODIS images and climate data, Remote Sens. Environ., 107, 510–519, doi:10.1016/j.rse.2006.10.003, 2007.

Li, Z., Tang, R., Wan, Z., Bi, Y., Zhou, C., Tang, B., Yan, G., and Zhang, X.: A review of current methodologies for regional evapotranspiration estimation from remotely sensed data, Sensors-Basel, 9, 3801–3853, doi:10.3390/s90503801, 2009.

Li, Z., Gao, Z., Gao, W., Shi, R., and Liu, C.: Spatio-temporal feature of land use/land cover dynamic changes in China from 1999 to 2009, T. Chin. Soc. Agr. Eng., 27, 312–322, 2011.

Li, Z. Q., Yu, G. R., Wen, X. F., Zhang, L. M., Ren, C. Y., and Fu, Y. L.: Energy balance closure at ChinaFLUX sites, Sci. China Ser. D, 48, 51–62, doi:10.1360/05zd0005, 2005.

Liu, J., Chen, J. M., Cihlar, J., and Park, W. M.: A process-based boreal ecosystem productivity simulator using remote sensing inputs, Remote Sens. Environ., 62, 158–175, 1997.

Liu, J., Chen, J. M., Cihlar, J., and Chen, W.: Net primary productivity distribution in the BOREAS region from a process model using satellite and surface data, J. Geophys. Res.-Atmos., 104, 27735–27754, 1999.

Liu, J., Chen, J. M., and Cihlar, J.: Mapping evapotranspiration based on remote sensing: An application to Canada's landmass, Water Resour. Res., 39, 1189, doi:10.1029/2002WR001680, 2003.

Liu, J. Y., Zhang, Q., and Hu, Y. F.: Regional differences of China's urban expansion from late 20th to early 21st century based on remote sensing information, Chin. Geogr. Sci., 22, 1–14, doi:10.1007/s11769-012-0510-8, 2012.

Liu, M. L., Tian, H. Q., Chen, G. S., Ren, W., Zhang, C., and Liu, J. Y.: Effects of land-use and land-cover change on evapotranspiration and water yield in China during 1900–2000, J. Am. Water Resour. Assoc., 44, 1193–1207, doi:10.1111/j.1752-1688.2008.00243.x, 2008.

Liu, M. L., Tian, H. Q., Lu, C. Q., Xu, X. F., Chen, G. S., and Ren, W.: Effects of multiple environment stresses on evapotranspiration and runoff over eastern China, J. Hydrol., 426, 39–54, doi:10.1016/j.jhydrol.2012.01.009, 2012.

Liu, R., Chen, J. M., Liu, J., Deng, F., and Sun, R.: Application of a new leaf area index algorithm to China's landmass using MODIS data for carbon cycle research, J. Environ. Manage., 85, 649–658, 2007.

Liu, S. and Gong, P.: Change of surface cover greenness in China between 2000 and 2010, Chinese Sci. Bull., 57, 2835–2845, doi:10.1007/s11434-012-5267-z, 2012.

Liu, Y., Yu, G., Wen, X., Wang, Y., Song, X., Li, J., Sun, X., Yang, F., Chen, Y., and Liu, Q.: Seasonal dynamics of CO_2 fluxes from subtropical plantation coniferous ecosystem, Sci. China Ser. D, 49, 99–109, doi:10.1007/s11430-006-8099-3, 2006.

Liu, Y., Ju, W., Chen, J., Zhu, G., Xing, B., Zhu, J., and He, M.: Spatial and temporal variations of forest LAI in China during 2000–2010, Chinese Sci. Bull., 57, 2846–2856, doi:10.1007/s11434-012-5064-8, 2012.

Liu, Y., Ju, W., He, H., Wang, S., Sun, R., and Zhang, Y.: Changes of net primary productivity in China during recent 11 years detected using an ecological model driven by MODIS data, Front. Earth Sci., 7, 112–127, doi:10.1007/s11707-012-0348-5, 2013.

Loveland, T. R. and Belward, A. S.: The IGBP-DIS global 1 km land cover data set, DISCover: First results, Int. J. Remote Sens., 18, 3289–3295, doi:10.1080/014311697217099, 1997.

Lu, E., Luo, Y., Zhang, R., Wu, Q., and Liu, L.: Regional atmospheric anomalies responsible for the 2009–2010 severe drought in China, J. Geophys. Res.-Atmos., 116, D21114, doi:10.1029/2011jd015706, 2011.

Ma, Z. and Fu, C.: Some evidence of drying trend over northern China from 1951 to 2004, Chinese Sci. Bull., 51, 2913–2925, doi:10.1007/s11434-006-2159-0, 2006.

Matsushita, B. and Tamura, M.: Integrating remotely sensed data with an ecosystem model to estimate net primary productivity in East Asia, Remote Sens. Environ., 81, 58–66, 2002.

Meehl, G. A. and Tebaldi, C.: More intense, more frequent, and longer lasting heat waves in the 21st century, Science, 305, 994–997, doi:10.1126/science.1098704, 2004.

Miralles, D. G., Holmes, T. R. H., De Jeu, R. A. M., Gash, J. H., Meesters, A. G. C. A., and Dolman, A. J.: Global land-surface evaporation estimated from satellite-based observations, Hydrol. Earth Syst. Sci., 15, 453–469, doi:10.5194/hess-15-453-2011, 2011.

Monteith, J. L.: Evaporation and the environment, Proc. Symp. Exp. Biol., 19, 205–234, 1965.

Mu, Q., Heinsch, F. A., Zhao, M., and Running, S. W.: Development of a global evapotranspiration algorithm based on MODIS and global meteorology data, Remote Sens. Environ., 111, 519–536, 2007.

Mu, Q., Zhao, M., Running, S. W., Liu, M., and Tian, H.: Contribution of increasing CO_2 and climate change to the carbon cycle in China's ecosystems, J. Geophys. Res.-Biogeo., 113, G01018, doi:10.1029/2006jg000316, 2008.

Mu, Q. Z., Zhao, M. S., and Running, S. W.: Improvements to a MODIS global terrestrial evapotranspiration algorithm, Remote Sens. Environ., 115, 1781–1800, 2011.

Mueller, B., Seneviratne, S. I., Jimenez, C., Corti, T., Hirschi, M., Balsamo, G., Ciais, P., Dirmeyer, P., Fisher, J. B., Guo, Z., Jung, M., Maignan, F., McCabe, M. F., Reichle, R., Reichstein, M., Rodell, M., Sheffield, J., Teuling, A. J., Wang, K., Wood, E. F., and Zhang, Y.: Evaluation of global observations-based evapotranspiration datasets and IPCC AR4 simulations, Geophys. Res. Lett., 38, doi:10.1029/2010gl046230, 2011.

Oki, T. and Kanae, S.: Global hydrological cycles and world water resources, Science, 313, 1068–1072, doi:10.1126/science.1128845, 2006.

Peng, S., Chen, A., Xu, L., Cao, C., Fang, J., Myneni, R. B., Pinzon, J. E., Tucker, C. J., and Piao, S.: Recent change of vegetation growth trend in China, Environ. Res. Lett., 6, 044027, doi:10.1088/1748-9326/6/4/044027, 2011.

Piao, S. L., Friedlingstein, P., Ciais, P., de Noblet-Ducoudre, N., Labat, D., and Zaehle, S.: Changes in climate and land use have a larger direct impact than rising CO_2 on global river runoff trends, P. Natl. Acad. Sci. USA, 104, 15242–15247, doi:10.1073/pnas.0707213104, 2007.

Piao, S. L., Yin, L., Wang, X. H., Ciais, P., Peng, S. S., Shen, Z. H., and Seneviratne, S. I.: Summer soil moisture regulated by precipitation frequency in China, Environ. Res. Lett., 4, 044012, doi:10.1088/1748-9326/4/4/044012, 2009.

Piao, S. L., Ciais, P., Huang, Y., Shen, Z. H., Peng, S. S., Li, J. S., Zhou, L. P., Liu, H. Y., Ma, Y. C., Ding, Y. H., Friedlingstein, P., Liu, C. Z., Tan, K., Yu, Y. Q., Zhang, T. Y., and Fang, J. Y.: The impacts of climate change on water resources and agriculture in China, Nature, 467, 43–51, 2010.

Piao, S. L., Ciais, P., Lomas, M., Beer, C., Liu, H. Y., Fang, J. Y., Friedlingstein, P., Huang, Y., Muraoka, H., Son, Y. H., and Woodward, I.: Contribution of climate change and rising CO_2 to terrestrial carbon balance in East Asia: A multi-model analysis, Global Planet. Change, 75, 133–142, 2011.

Piao, S. L., Ito, A., Li, S. G., Huang, Y., Ciais, P., Wang, X. H., Peng, S. S., Nan, H. J., Zhao, C., Ahlström, A., Andres, R. J., Chevallier, F., Fang, J. Y., Hartmann, J., Huntingford, C., Jeong, S., Levis, S., Levy, P. E., Li, J. S., Lomas, M. R., Mao, J. F., Mayorga, E., Mohammat, A., Muraoka, H., Peng, C. H., Peylin, P., Poulter, B., Shen, Z. H., Shi, X., Sitch, S., Tao, S., Tian, H. Q., Wu, X. P., Xu, M., Yu, G. R., Viovy, N., Zaehle, S., Zeng, N., and Zhu, B.: The carbon budget of terrestrial ecosystems in East Asia over the last two decades, Biogeosciences, 9, 3571–3586, doi:10.5194/bg-9-3571-2012, 2012.

Pisek, J., Chen, J. M., and Deng, F.: Assessment of a global leaf area index product from SPOT-4 VEGETATION data over selected sites in Canada, Can. J. Remote Sens., 33, 341–356, 2007.

Potter, C. S., Wang, S. S., Nikolov, N. T., McGuire, A. D., Liu, J., King, A. W., Kimball, J. S., Grant, R. F., Frolking, S. E., Clein, J. S., Chen, J. M., and Amthor, J. S.: Comparison of boreal ecosystem model sensitivity to variability in climate and forest site parameters, J. Geophys. Res.-Atmos., 106, 33671–33687, doi:10.1029/2000jd000224, 2001.

Qin, N., Chen, X., Fu, G., Zhai, J., and Xue, X.: Precipitation and temperature trends for the Southwest China: 1960–2007, Hydrol. Process., 24, 3733–3744, doi:10.1002/hyp.7792, 2010.

Qin, Z., Yu, Q., Xu, S. H., Hu, B. M., Sun, X. M., Liu, E. M., Wang, J. S., Yu, G. R., and Zhu, Z. L.: Water, heat fluxes and water use efficiency measurement and modeling above a farmland in the North China Plain, Sci. China Ser. D, 48, 207–217, 2005.

Rodell, M., McWilliams, E. B., Famiglietti, J. S., Beaudoing, H. K., and Nigro, J.: Estimating evapotranspiration using an observation based terrestrial water budget, Hydrol. Process., 25, 4082–4092, doi:10.1002/hyp.8369, 2011.

Ryu, Y., Baldocchi, D. D., Ma, S., and Hehn, T.: Interannual variability of evapotranspiration and energy exchange over an annual grassland in California, J. Geophys. Res.-Atmos., 113, D09104, doi:10.1029/2007jd009263, 2008.

Ryu, Y., Baldocchi, D. D., Kobayashi, H., van Ingen, C., Li, J., Black, T. A., Beringer, J., van Gorsel, E., Knohl, A., Law, B. E., and Roupsard, O.: Integration of MODIS land and atmosphere products with a coupled-process model to estimate gross primary productivity and evapotranspiration from 1 km to global scales, Global Biogeochem. Cy., 25, GB4017, doi:10.1029/2011gb004053, 2011.

Sahoo, A. K., Pan, M., Troy, T. J., Vinukollu, R. K., Sheffield, J., and Wood, E. F.: Reconciling the global terrestrial water budget using satellite remote sensing, Remote Sens. Environ., 115, 1850–1865, doi:10.1016/j.rse.2011.03.009, 2011.

Sasai, T., Saigusa, N., Nasahara, K. N., Ito, A., Hashimoto, H., Nemani, R., Hirata, R., Ichii, K., Takagi, K., Saitoh, T. M., Ohta, T., Murakami, K., Yamaguchi, Y., and Oikawa, T.: Satellite-driven estimation of terrestrial carbon flux over Far East Asia with 1-km grid resolution, Remote Sens. Environ., 115, 1758–1771, doi:10.1016/j.rse.2011.03.007, 2011.

Saxton, K. E., Rawls, W. J., Romberger, J. S., and Papendick, R. I.: Estimating generalized soil-water characteristics from texture, Soil. Sci. Soc. Am. J., 50, 1031–1036, 1986.

Schaefer, K., Schwalm, C. R., Williams, C., Arain, M. A., Barr, A., Chen, J. M., Davis, K. J., Dimitrov, D., Hilton, T. W., Hollinger, D. Y., Humphreys, E., Poulter, B., Raczka, B. M., Richardson, A. D., Sahoo, A., Thornton, P., Vargas, R., Verbeeck, H., Anderson, R., Baker, I., Black, T. A., Bolstad, P., Chen, J., Curtis, P. S., Desai, A. R., Dietze, M., Dragoni, D., Gough, C., Grant, R. F., Gu, L., Jain, A., Kucharik, C., Law, B., Liu, S., Lokipitiya, E., Margolis, H. A., Matamala, R., McCaughey, J. H., Monson, R., Munger, J. W., Oechel, W., Peng, C., Price, D. T., Ricciuto, D., Riley, W. J., Roulet, N., Tian, H., Tonitto, C., Torn, M., Weng, E., and Zhou, X.: A model-data comparison of gross primary productivity: Results from the North American Carbon Program site synthesis, J. Geophys. Res.-Biogeo., 117, G03010, doi:10.1029/2012jg001960, 2012.

Schwalm, C. R., Williams, C. A., Schaefer, K., Anderson, R., Arain, M. A., Baker, I., Barr, A., Black, T. A., Chen, G., Chen, J. M., Ciais, P., Davis, K. J., Desai, A., Dietze, M., Dragoni, D., Fischer, M. L., Flanagan, L. B., Grant, R., Gu, L., Hollinger, D., Izaurralde, R. C., Kucharik, C., Lafleur, P., Law, B. E., Li, L., Li, Z., Liu, S., Lokupitiya, E., Luo, Y., Ma, S., Margolis, H., Matamala, R., McCaughey, H., Monson, R. K., Oechel, W. C., Peng, C., Poulter, B., Price, D. T., Riciutto, D. M., Riley, W., Sahoo, A. K., Sprintsin, M., Sun, J., Tian, H., Tonitto, C., Verbeeck, H., and Verma, S. B.: A model-data intercomparison of

CO$_2$ exchange across North America: Results from the North American Carbon Program site synthesis, J. Geophys. Res., 115, G00H05, doi:10.1029/2009jg001229, 2010.

Sellers, P. J., Randall, D. A., Collatz, G. J., Berry, J. A., Field, C. B., Dazlich, D. A., Zhang, C., Collello, G. D., and Bounoua, L.: A revised land surface parameterization (SiB2) for atmospheric GCMs, Part I: Model formulation, J. Climate, 9, 676-705, 1996.

Seneviratne, S. I., Corti, T., Davin, E. L., Hirschi, M., Jaeger, E. B., Lehner, I., Orlowsky, B., and Teuling, A. J.: Investigating soil moisture-climate interactions in a changing climate: A review, Earth-Sci. Rev., 99, 125–161, doi:10.1016/j.earscirev.2010.02.004, 2010.

Shangguan, W., Dai, Y., Liu, B., Ye, A., and Yuan, H.: A soil particle-size distribution dataset for regional land and climate modelling in China, Geoderma, 171–172, 85–91, doi:10.1016/j.geoderma.2011.01.013, 2012.

Sonnentag, O., Chen, J. M., Roulet, N. T., Ju, W., and Govind, A.: Spatially explicit simulation of peatland hydrology and carbon dioxide exchange: Influence of mesoscale topography, J. Geophys. Res.-Biogeo., 113, G02005, doi:10.1029/2007JG000605, 2008.

Sprintsin, M., Chen, J. M., Desai, A., and Gough, C. M.: Evaluation of leaf-to-canopy upscaling methodologies against carbon flux data in North America, J. Geophys. Res.-Biogeo., 117, G01023, doi:10.1029/2010jg001407, 2012.

Su, Z.: The Surface Energy Balance System (SEBS) for estimation of turbulent heat fluxes, Hydrol. Earth Syst. Sci., 6, 85–100, doi:10.5194/hess-6-85-2002, 2002.

Sun, G., McNulty, S. G., Lu, J., Amatya, D. M., Liang, Y., and Kolka, R. K.: Regional annual water yield from forest lands and its response to potential deforestation across the southeastern United States, J. Hydrol., 308, 258–268, doi:10.1016/j.jhydrol.2004.11.021, 2005.

Sun, G., Zhou, G. Y., Zhang, Z. Q., Wei, X. H., McNulty, S. G., and Vose, J. M.: Potential water yield reduction due to forestation across China, J. Hydrol., 328, 548–558, doi:10.1016/j.jhydrol.2005.12.013, 2006.

Sun, R., Chen, J. M., Zhu, Q. J., Zhou, Y. Y., Liu, J., Li, J. T., Liu, S. H., Yan, G. J., and Tang, S. H.: Spatial distribution of net primary productivity and evapotranspiration in Changbaishan Natural Reserve, China, using Landsat ETM+ data, Can. J. Remote Sens., 30, 731–742, 2004.

Trenberth, K. E., Jones, P. D., Ambenje, P., Bojariu, R., Easterling, D., Klein Tank, A., Parker, D., Rahimzadeh, F., Renwick, J. A., Rusticucci, M., Soden, B., and Zhai, P.: Observations: Surface and Atmospheric Climate Change, in: Climate Change 2007: The Physical Science Basis, Contribution of Working Group I to the Fourth Assessment Report of the Intergovernmental Panel on Climate Change, edited by: Solomon, S., Qin, D., Manning, M., Chen, Z., Marquis, M., Averyt, K. B., Tignor, M., and Miller, H. L., Cambridge University Press, Cambridge, UK and New York, NY, USA, 2007.

Trenberth, K. E., Fasullo, J. T., and Kiehl, J.: Earth's global energy budget, B. Am. Meteorol. Soc., 90, 311–323, doi:10.1175/2008bams2634.1, 2009.

Twine, T. E., Kucharik, C. J., and Foley, J. A.: Effects of land cover change on the energy and water balance of the Mississippi River basin, J. Hydrometeorol., 5, 640–655, doi:10.1175/1525-7541(2004)005<0640:eolcco>2.0.co;2, 2004.

Verstraeten, W. W., Veroustraete, F., and Feyen, J.: Assessment of evapotranspiration and soil moisture content across different scales of observation, Sensors-Basel, 8, 70–117, doi:10.3390/s8010070, 2008.

Vinukollu, R. K., Wood, E. F., Ferguson, C. R., and Fisher, J. B.: Global estimates of evapotranspiration for climate studies using multi-sensor remote sensing data: Evaluation of three process-based approaches, Remote Sens. Environ., 115, 801–823, 2011.

Wang, A. H., Lettenmaier, D. P., and Sheffield, J.: Soil Moisture Drought in China, 1950–2006, J. Climate, 24, 3257–3271, 2011.

Wang, K. and Dickinson, R. E.: A review of global terrestrial evapotranspiration: observation, modeling, climatology, and climatic variability, Rev. Geophys., 50, Rg2005, doi:10.1029/2011rg000373, 2012.

Wang, K. and Liang, S.: An improved method for estimating global evapotranspiration based on satellite determination of surface net radiation, vegetation index, temperature, and soil moisture, J. Hydrometeor., 9, 712–727, doi:10.1175/2007jhm911.1, 2008.

Wang, K., Dickinson, R. E., Wild, M., and Liang, S.: Evidence for decadal variation in global terrestrial evapotranspiration between 1982 and 2002: 2. Results, J. Geophys. Res.-Atmos., 115, D20113, doi:10.1029/2010jd013847, 2010.

Wang, L., Li, C., Ying, Q., Cheng, X., Wang, X., Li, X., Hu, L., Liang, L., Yu, L., Huang, H., and Gong, P.: China's urban expansion from 1990 to 2010 determined with satellite remote sensing, Chinese Sci. Bull., 57, 2802–2812, doi:10.1007/s11434-012-5235-7, 2012.

Wang, Q., Tenhunen, J., Falge, E., Bernhofer, C., Granier, A., and Vesala, T.: Simulation and scaling of temporal variation in gross primary production for coniferous and deciduous temperate forests, Global Change Biol., 10, 37–51, 2004.

Wang, Q. F., Niu, D., Yu, G. R., Ren, C. Y., Wen, X. F., Chen, J. M., and Ju, W. M.: Simulating the exchanges of carbon dioxide, water vapor and heat over Changbai Mountains temperate broadleaved Korean pine mixed forest ecosystem, Sci. China Ser. D, 48, 148–159, doi:10.1360/05zd0015, 2005.

Wen, X., Yu, G., Sun, X., Li, Q., Ren, C., and Han, S.: Net water vapour exchange over a mixed needle and broad-leaved forest in Changbai Mountain during autumn, J. Geogr. Sci., 13, 463–468, 2003.

Wen, X. F., Yu, G. R., Sun, X. M., Li, Q. K., Liu, Y. F., Zhang, L. M., Ren, C. Y., Fu, Y. L., and Li, Z. Q.: Soil moisture effect on the temperature dependence of ecosystem respiration in a subtropical Pinus plantation of southeastern China, Agr. Forest Meteorol., 137, 166–175, 2006.

Xiao, J., Sun, G., Chen, J., Chen, H., Chen, S., Dong, G., Gao, S., Guo, H., Guo, J., Han, S., Kato, T., Li, Y., Lin, G., Lu, W., Ma, M., McNulty, S., Shao, C., Wang, X., Xie, X., Zhang, X., Zhang, Z., Zhao, B., Zhou, G., and Zhou, J.: Carbon fluxes, evapotranspiration, and water use efficiency of terrestrial ecosystems in China, Agr. Forest Meteorol., 182–183, 76–90, doi:10.1016/j.agrformet.2013.08.007, 2013.

Yan, H., Wang, S. Q., Billesbach, D., Oechel, W., Zhang, J. H., Meyers, T., Martin, T. A., Matamala, R., Baldocchi, D., Bohrer, G., Dragoni, D., and Scott, R.: Global estimation of evapotranspiration using a leaf area index-based surface energy and water balance model, Remote Sens. Environ., 124, 581–595, doi:10.1016/j.rse.2012.06.004, 2012.

Yang, Y., Shang, S., and Jiang, L.: Remote sensing temporal and spatial patterns of evapotranspiration and the responses to water management in a large irrigation district of North China, Agr. Forest Meteorol., 164, 112–122, doi:10.1016/j.agrformet.2012.05.011, 2012.

Yao, Y., Liang, S., Cheng, J., Liu, S., Fisher, J. B., Zhang, X., Jia, K., Zhao, X., Qin, Q., Zhao, B., Han, S., Zhou, G., Zhou, G., Li, Y., and Zhao, S.: MODIS-driven estimation of terrestrial latent heat flux in China based on a modified Priestley–Taylor algorithm, Agr. Forest Meteorol., 171–172, 187–202, doi:10.1016/j.agrformet.2012.11.016, 2013.

Yu, D. Y., Shi, P. J., Han, G. Y., Zhu, W. Q., Du, S. Q., and Xun, B.: Forest ecosystem restoration due to a national conservation plan in China, Ecol. Eng., 37, 1387–1397, doi:10.1016/j.ecoleng.2011.03.011, 2011.

Yu, G. R., Wen, X. F., Sun, X. M., Tanner, B. D., Lee, X. H., and Chen, J. Y.: Overview of ChinaFLUX and evaluation of its eddy covariance measurement, Agr. Forest Meteorol., 137, 125–137, 2006.

Yu, P., Krysanova, V., Wang, Y., Xiong, W., Mo, F., Shi, Z., Liu, H., Vetter, T., and Huang, S.: Quantitative estimate of water yield reduction caused by forestation in a water-limited area in northwest China, Geophys. Res. Lett., 36, L02406, doi:10.1029/2008gl036744, 2009.

Yuan, W. P., Liu, S. G., Yu, G. R., Bonnefond, J. M., Chen, J. Q., Davis, K., Desai, A. R., Goldstein, A. H., Gianelle, D., Rossi, F., Suyker, A. E., and Verma, S. B.: Global estimates of evapotranspiration and gross primary production based on MODIS and global meteorology data, Remote Sens. Environ., 114, 1416–1431, doi:10.1016/j.rse.2010.01.022, 2010.

Zeng, Z. Z., Piao, S. L., Lin, X., Yin, G. D., Peng, S. S., Ciais, P., and Myneni, R. B.: Global evapotranspiration over the past three decades: estimation based on the water balance equation combined with empirical models, Environ. Res. Lett., 7, 014026, doi:10.1088/1748-9326/7/1/014026, 2012.

Zhang, F., Ju, W., Chen, J., Wang, S., Yu, G., Li, Y., Han, S., and Asanuma, J.: Study on evapotranspiration in East Asia using the BEPS ecological model, J. Nat. Resour., 25, 1596–1606, 2010.

Zhang, F., Chen, J. M., Chen, J., Gough, C. M., Martin, T. A., and Dragoni, D.: Evaluating spatial and temporal patterns of MODIS GPP over the conterminous U.S. against flux measurements and a process model, Remote Sens. Environ., 124, 717–729, doi:10.1016/j.rse.2012.06.023, 2012a.

Zhang, F., Ju, W., Shen, S., Wang, S., Yu, G., and Han, S.: Variations of terrestrial net primary productivity in East Asia, Terr. Atmos. Ocean Sci., 23, 425–437, doi:10.3319/tao.2012.03.28.01(a), 2012b.

Zhang, K., Kimball, J. S., Mu, Q. Z., Jones, L. A., Goetz, S. J., and Running, S. W.: Satellite based analysis of northern ET trends and associated changes in the regional water balance from 1983 to 2005, J. Hydrol., 379, 92–110, doi:10.1016/j.jhydrol.2009.09.047, 2009.

Zhang, K., Kimball, J. S., Nemani, R. R., and Running, S. W.: A continuous satellite-derived global record of land surface evapotranspiration from 1983 to 2006, Water Resour. Res., 46, W09522, doi:10.1029/2009wr008800, 2010.

Zhang, L., Dawes, W. R., and Walker, G. R.: Response of mean annual evapotranspiration to vegetation changes at catchment scale, Water Resour. Res., 37, 701–708, doi:10.1029/2000wr900325, 2001.

Zhang, M., Yu, G. R., Zhuang, J., Gentry, R., Fu, Y. L., Sun, X. M., Zhang, L. M., Wen, X. F., Wang, Q. F., Han, S. J., Yan, J. H., Zhang, Y. P., Wang, Y. F., and Li, Y. N.: Effects of cloudiness change on net ecosystem exchange, light use efficiency, and water use efficiency in typical ecosystems of China, Agr. Forest Meteorol., 151, 803–816, 2011a.

Zhang, Q., Xu, C.-Y., Chen, Y. D., and Ren, L.: Comparison of evapotranspiration variations between the Yellow River and Pearl River basin, China, Stoch. Env. Res. Risk A, 25, 139–150, doi:10.1007/s00477-010-0428-6, 2011b.

Zhang, Y. Q. and Wegehenkel, M.: Integration of MODIS data into a simple model for the spatial distributed simulation of soil water content and evapotranspiration, Remote Sens. Environ., 104, 393–408, 2006.

Zhang, Y. Q., Leuning, R., Chiew, F. H. S., Wang, E. L., Zhang, L., Liu, C. M., Sun, F. B., Peel, M. C., Shen, Y. J., and Jung, M.: Decadal trends in evaporation from global energy and water balances, J. Hydrometeorol., 13, 379–391, doi:10.1175/jhm-d-11-012.1, 2012.

Zhao, M. and Running, S. W.: Drought-induced reduction in global terrestrial net primary production from 2000 through 2009, Science, 329, 940–943, doi:10.1126/science.1192666, 2010.

Zhou, L., Wang, S., Chen, J., Feng, X., Ju, W., and Wu, W.: The spatial-temporal characteristics of evapotranspiration of China's terrestrial ecosystems during 1991–2000, Resour. Sci., 31, 962–972, 2009.

Zhu, Q. A., Jiang, H., Liu, J. X., Wei, X. H., Peng, C. H., Fang, X. Q., Liu, S. R., Zhou, G. M., Yu, S. Q., and Ju, W. M.: Evaluating the spatiotemporal variations of water budget across China over 1951–2006 using IBIS model, Hydrol. Process., 24, 429–445, 2010.